UiT
THE ARCTIC UNIVERSITY OF NORWAY

Faculty of Engineering Science and Technology

Wind turbines and ice breaking

Understanding of the mechanical properties of ice and the forces acting on the wind turbine blade and ice shape. Also, a general understanding on the processes involved for ice breaking and shedding.

Peter Tor Furseth Nilsen

Master thesis in Engineering Design Spring 2019

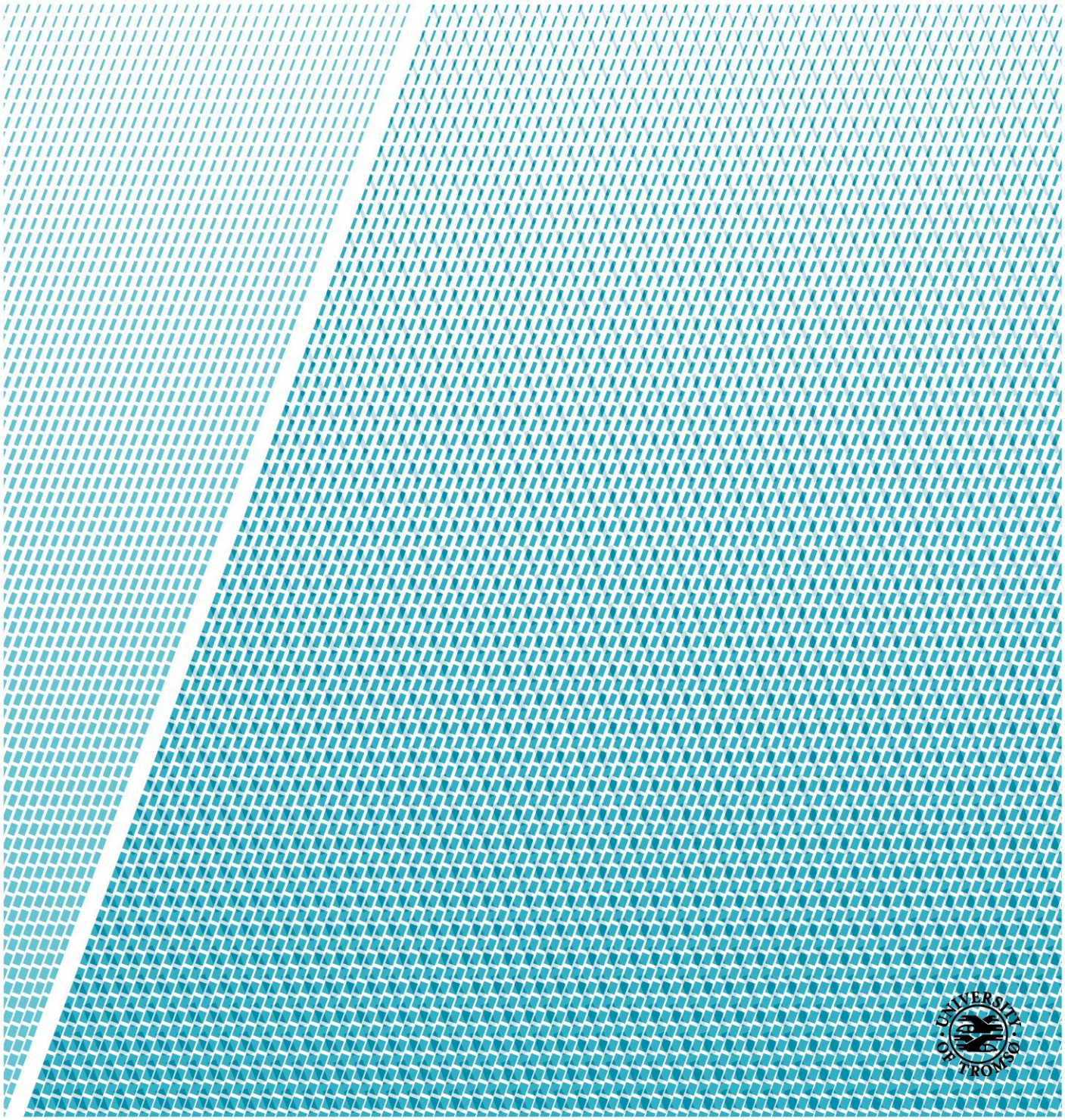

Acknowledgment

This report concludes a five-year education with a master degree in an engineering direction that builds on mechanical engineering. An education that has been both very challenging but also rewarding. With this education, it is time to take the next step in life and from there, see what the future will bring.

First, I want to thank Nordkraft Vind and Dr. Matthew Carl Homola for the assignment, and Mr. Homola for his contribution as a supervisor.

In addition, I want to thank Dr. Per Johan Nicklasson, Dr. Guy Beeri Mauseth and Harpal Singh, who were supervisor from UiT The Arctic University of Norway in Narvik. Throughout the last semester writing this thesis, I have had several meetings with Dr. Nicklasson, Dr. Mauseth and Mr. Singh. In those meetings I have received lot feedback, ideas and help, but also great encouragement, which have given me a motivational boost when needed.

Peter Tor Furseth Nilsen

Narvik, June 7, 2019

Abstract

With increasing focus on renewable energy development of new wind turbine parks have grown over the last decade. Norway and the Nordic region are of good interest for this development due to benefit such as; low development cos, good wind resources, stable political system, solid power grids and space to build on a large scale. However, the arctic climate imposes the challenge of ice accretion on the blades of the wind turbine created by the atmospheric ice. Over time, the ice build-up causes ice shedding which can do structural damage to the wind turbine. The process involving ice breaking and shedding is not well understood. This document explains the mechanical properties of ice such as density, coefficient of thermal expansion, elastic modulus and structural build-up of ice.

On how ice sticks to the blade surface for a wind turbine, adhesive properties for ice is explained. By previous study of adhesive properties of ice, shear forces and tension forces has been tested to find the adhesive shear strength and tension.

In understanding of ice breaking, ice deformation is explained on how ice deforms elastically, plastically and by brittle fracture. In addition, creep is briefly explained due to the influential factors for deformation are the same, all though creep is not a reason for ice shedding. The properties of ice failure are mentioned as well as the three regimes; ductile, transitional and brittle regime. The brittle regime of ice failure are further split into three categories; intermittent, lock-in and continuous brittle crushing. This is based on the speed range of development of ice force and the structure response.

Simulations are done to understand how deflection, as well as lift and drag, acts for the blade in regards of wind direction and gravitational force. For this a model of a wind turbine blade is made in Inventor and analyzed in Ansys. To achieve good estimated results from the analysis appropriate material selection is necessary. An understanding of what materials is used for wind turbine blades is mentioned with its desired properties and build-up.

Table of Contents

List of Figures

List of Tables

1. Introduction

During the last decade the use of renewable energy has had a significant growth. The European Union has set as a goal to reduce climate gasses by 20% and increase the use renewable energy by 20% by 2020 [1]. Looking at wind power, the global investment has increased from 20 billion dollars to 107 billion dollars [2]. Wind power is one of the most environmental friendly power generation in large scale energy production that is available today [1].

From 1993 to 2017 the wind power generation in Norway has grown from 7 GWh to 2,900 Gwh. In 2018 wind power generation from January to June has increased by 35% from 2017 in the same period [3]. The growth of wind power really took off in Norway in 2011 due to lower interest rates and foreign investment in Norwegian and Nordic wind energy. According to the investment director for Asper, Allister Sykes, the Nordic region is one of the most attractive geographies. This due to benefits like low development costs, good wind resources, stabile political systems, solid power grids and space to build in a large scale. Asper specializes in investments in renewable energy and has a large investment in Swedish wind power [4]. Other benefits mentioned for investments in the Nordic wind industry is because it is modern with professional developers, advisors and banks.

1.1. Purpose of the study

Due to the cold environment at places wind turbines are placed, atmospheric ice can form on the wind turbine blades. This ice breaks and falls off, but the process involved in the ice breaking and shedding is not well understood. This project shall document the mechanical properties of ice and the forces acting on the wind turbine blade and the ice shape. The project shall describe what stress will result in ice breaking for different ice thickness. The goal of the project is to determine an estimate of the maximum ice thickness that will occur before ice breaking and shedding becomes likely.

1.2. Limitations

Due to differences in wind turbine blades, environments and climate, a general understanding of ice breaking and shedding is the area of focus. The model made of the wind turbine blade will be a simplified design with load put on for simulation analysis.

The blade twisting and the aerodynamic forces acting on the ice shape may be neglected. Also, forces due to unsteady nature of the wind may be neglected. These two topics have a secondary priority due to the projects total workload.

Today, there are mainly two types of wind turbines; horizontal-axis turbines (HAWT) and vertical-axis turbines (VAWT). HAWTs are built with a large tower, where blades are mounted on the top of the tower. The blades are similar to airplane propellers and there are usually three blades [5].

VAWTs are not as sensitive to wind direction and turbulence and can therefore be mounted closer to the ground making them cheaper to build and maintain. VAWT comes in a variety of shapes and sizes. What is common for VAWT blades, is that they are mounted vertically from the lower part of the wind tower to the upper part [6].

Figure 1: To the left a horizontal-axis wind turbine [42] and to the right a Darrieus vertical-axis wind turbine [43].

The project was given by Nordkraft Vind Narvik, which has a wind farm with 14 wind turbines at Nygårdsfjellet. These wind turbines are HAWTs, and therefore those turbines will be focused on while VAWT are excluded from this rapport.

As for standards, by searching for “Vindturbin” on standard.no, a database for standards that are applied in Norway, three results were found; NEK EN 61400-21:2002, NEK EN 81346-1/-2:2009 and NS 3457-3:2013. For more results concerning wind turbines, a search was done at the ANSI online web store. ANSI stands for American National Standard Institute. However, since the standard are precautionary and not relevant to this project, the standards are neglected.

The report itself should not exceed 50 pages. This excludes the appendices.

1.3. Expected outcome

The documentation shall give an understanding of the mechanical properties of ice and the forces acting on the wind turbine blade and ice shape. Also, it should give a general understanding of the processes involved in ice breaking and shedding.

Previous work indicate that ice shedding is presumably due to tensile failure in the ice. Tensile strength of atmospheric ice is, by indications, its weakest property. By further investigation of the ice stresses that occur in the two main directions, forward/back and up/down, the report should give an understanding of how these stresses affect ice cracking.

There are three ranges of motion/stress sources that should be described:

- Force differences occurring cyclically during the rotation of the rotor.
- Force differences between steady-state operation and idling rotor.

2. Understanding of ice

To understand ice shedding, it is important to have an understanding of different factors of ice. This section focus on what icing is and its build up depending on what parameter there are controlling atmospheric icing, the characteristics of ice, what problems ice accretion causes the wind turbine and its energy production, the properties and mechanics of ice, deformation and failure of ice as well as the mechanisms of ice accretion and ablation. Properties such as the elastic modulus, shear modulus, density and the adhesive properties of ice is elaborated on to help getting an insight of ice breaking and shedding.

2.1. Forming of icing

Icing forms when water in form of snow, fog, cloud or rain comes in contact with an exposed surface at temperature below freezing point for water. Atmospheric icing is the term used to describe ice accretion on structures or objects. Based on the two formation processes, atmospheric icing can be classified as [7]:

- **Precipitation icing** is formed due to wet snow or freezing rain/drizzle.
- **In-cloud icing** happens when clouds with supercooled liquid collides with structures or objects and freezes.

The icing result of precipitation icing is either glaze ice or wet snow, where both has a strong adhesion force when fully frozen. Adhesion is the property of different molecules or surfaces to cling to each other. From studies, glaze ice thrown has been recorded with within distance of 92 m from the turbine. However, for wet snow, indications shows that it falls directly of the turbine blade rather than being thrown. This suggest that wet snow may shed almost instantly.

Icing results from in-cloud icing are glaze ice, hard rime or soft rime which are determined by parameters like; ambient temperature, wind speed, heat flux of the surface etc. [8].

Parameters such as compression, shear strength, humidity, temperature and duration of ice accretions describe the nature of the accreted ice. The variation of meteorological conditions during ice growth will determine physical properties and appearance of the ice accretion. The density of ice accretion is decided by air temperature and wind speed and varies from low, medium to high density as shown in Figure 2 [7].

Table 1: Meteorological parameters controlling atmospheric ice accretion [8].

Type of ice	Air temperature [°C]	Wind speed [m/s]	Droplet size	Water content in air	Storm duration
Precipitation icing					
Glaze	$-10 < t_a < 0$	any	large	medium	hours
Wet snow	$0 < t_a < 3$	any	flakes	very high	hours
In-cloud icing					
Glaze	see Figure 2	see Figure 2	medium	high	hours
Hard rime	see Figure 2	see Figure 2	medium	medium	days
Soft rime	see Figure 2	see Figure 2	small	low	days

Ice accretion is referred to glaze, rime, wet snow and hoar frost.

Glaze is an ice coating formed by supercooled rain, drizzle or fog that impinges a surface with temperature below the freezing point. The accumulated water that covers the surface freezes relatively slowly and forms an ice accretion that is denser, harder and more transparent than other forms of accumulated ice [9].

Rime is the most common in-cloud icing and is divided into soft and hard rime. Soft rime forms when water vapor first condensate on a surface and then freezes immediately [10]. Hard rime is formed by small sized droplets that freezes almost immediately on impact of an object.

Wet snow occurs when the temperature is just above the freezing point and the snow crystals are partly melted. When wet snow comes in contact with an object and freezes, the ice will be weak due to partially unfrozen water [11].

Hoar frost is ice crystals formed by water vapor transition into ice caused by a direct phase transition. It has a low density and strength and rarely results in significant load of structures, and therefor normally neglected [7].

Meteorological conditions decides which type of ice accretion that occurs on the wind turbine blade, and with what characteristics as given in Table 2.

Table 2: Ice characteristics.

Type of ice	**Density [kg/m^3]**	**Adhesion/Cohesion**	**Color**	**Shape**
Glaze	900	Strong	Transparent	Evenly distributed/icicles
Rime, hard	600 – 900	Strong	Opaque	Eccentric, pointed windward
Rime, soft	200 – 600	Low to medium	White	Eccentric, pointed windward
Wet snow	300 – 600	Weak/strong	White	Evenly distributed/eccentric

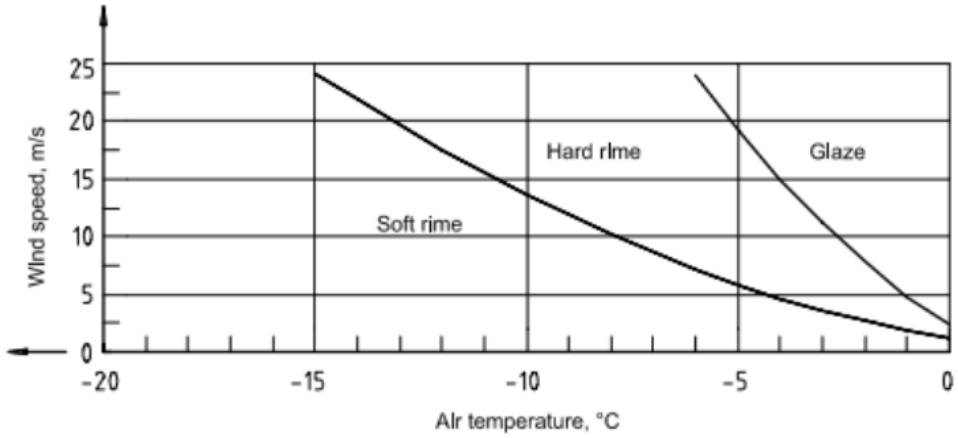

Figure 2: Density of ice accretion based on wind speed and temperature [7].

It is important to note that the heat flux on the surface of a wind turbine blade can affect the growth regime of ice and what type of ice deposits that forms. If all droplets freezes on impact, hard and soft rimes forms since the freezing fraction is in unity. This is known as the "dry growth" regime. The icing process gets complicated if the freezing fraction is less than unity. The general hypothesis is that there exist a thin water film on the surface of the object called "runback". Runback leads to a wet growth regime which results in glaze ice or mixed ice.

There are several parameters that affect the wet growth regime, such as heat flux of the surface, the heat transfer coefficient of the surface, true air speed, roughness of the surface and ice deposits. In addition, the heat transfer coefficient is a function of boundary layer effects and the

boundary layer itself is affected by true air speed and roughness of the surface. This makes any analytical modeling of the phenomenon highly complicated.

True air speed takes into consideration not only the velocity of inflowing air, but also the rotational motion of the wind turbine blade.

2.2. Problems due to ice accretions

During the last two decades there has been a tremendous growth of wind turbines, both inland and offshore. To utilize the wind turbines at their best potential, the location is very important for utilization of the wind resources. Places where wind turbine plants are installed, often make them exposed to periodically atmospheric icing.

Icing on wind turbines have a negative effect on their performance. An estimation of production loss on wind turbines in Aapua, Sweden, was approximately 25% due to icing alone during the winter season of 2009-2010 [10]. Icing on wind turbines causes a variety of problems; reduction of power production, overloading due to delayed stall, increased fatigue of components and risk of ice throw.

Ice accretion is due to cohesion and adhesion of water molecules. Cohesion is the property of equal molecules, or of the same substance, to stick to each other due to mutual attraction [12]. Water is the most important adhesive substance on Earth and is highly polar. One part of the molecule has a slightly negative charge, while the other has a slightly positive charge. This is due to the fact that nucleus of water's oxygen atom attracts the molecule's electrons more strongly than the nuclei of its hydrogen atoms. This allows water to interact with any other charged or polar substance [13]. Of non-metallic liquids, water is the most cohesive and this makes water clump into drops. What makes water molecules stick to each other is the positive and negative charge of hydrogen and oxygen atoms, which attracts to each other [14].

2.2.1. Reduction of power production

When wind hits the turbine blades, the energy of the wind makes the blade rotate. To extract the energy, the wind turbines slow down the wind. Ice accretion causes changes of the air flow and limits the effect of the wing's aerodynamic performance. The ice that forms on the leading

edge of the blade reduces the torque and changes the turbine's capability to utilize the energy of the wind [10]. Icing reduces the lift coefficient C_l [-] and increases the drag coefficient C_d [-], and this aerodynamic change can by expressed by

$$F_y = (C_l \cos(\beta) - C_d \sin(\beta)) \frac{1}{2} \rho v^2 c(r)$$

where ρ [kg/m^3] is air density, v [m/s] is air velocity relative to a point on the rotating blade, β [rad] is the inflow angle of the relative air velocity and c [m] is the chord length at radius r [m], [15].

2.2.2. **Overloading due to delayed stall**

Drag of ice prevents the turbine from reaching rated power. The turbine will then operate at a higher angle of attack and if not a stall occur, some portion of the wind turbine can overload due to a combination of drag and torque [15].

2.2.3. **Increase of fatigue of components**

Ice accretions on the wind turbine blades causes an imbalance in the rotor, due to added mass and aerodynamics. This increases the loads imposed on components of the wind turbine which shortens their lifespan [15].

2.2.4. **Ice shedding**

With the increase of wind parks, there is an increase of the possibility of personnel harm. This risk is greatest among service personnel. In the future other people may be at risk if wind parks are placed closer to roads and recreation areas. Ice pieces shed from the blades can be large and do significant damages. The equation

$$d = 1{,}5(D + H)$$

gives a rough estimate of which area is at risk of ice throw. d [m] is the possible length ice can be thrown, D [m] is the diameter of the rotor and H [m] is the height of the nacelle [15].

2.3. Ice Properties and mechanics

At temperature 0°C and atmospheric pressure 1 atm, the density of pure ice is 0.9168 g/cm^3, the specific volume is 1.0908 cm^3/g and the compressibility factor is approximately $(1-5)\cdot 10^{-5}$ per atm. However, the density differs slightly due to pores and impurities in the ice. Pressure may also exert a substantial influence on the density of porous ice, reducing the porosity and correspondingly increasing the density.

The coefficient of thermal expansion of ice is a function of temperature. The coefficient of linear expansion in the temperature range of -20°C to 0°C is on average $5.5\cdot 10^{-5}$ per °C, while in the temperature range of -40°C to -20°C the coefficient of linear expansion is about $3.6\cdot 10^{-5}$ per °C.

The specific heat of ice varies with the temperature and is expressed as

$$C_{ice} = 0.05057 - 0.001863\cdot\theta \text{ cal/g °C}$$

where θ [°C] is the absolute value of the negative temperature of ice. The latent heat fusion of pure ice is 79.6 cal/g, and for sublimation of ice at 0°C it is 677 cal/g. The thermal conductivity of ice is a function of the ice temperature and the coefficient of thermal conductivity of dense ice is a function of temperature and is expressed as

$$\lambda_{ice} = 0{,}0053(1+0{,}0015\cdot\theta) \text{ cal/cm sec °C}$$

where θ [°C] is the absolute value of the ice temperature. The elastic modulus characterize the resistance of a material to elastically deform in tension or compression and is expressed by the formula

$$E = \varepsilon\sigma$$

where E [N/mm^2] is the elastic modulus, σ [N/mm^2] is the normal stress and ε [-] is the strain. In tension, the elastic modulus is also the coefficient which connects the normal tensile stress with the relative elongation. For a material the deformation normally disappears when the force that is acting on it is removed. There are different factors that affects the elastic modulus and makes it, to a certain extent indeterminable, since it is difficult to distinguish the purely elastic deformation. V. N. Pinegin [16] showed that the elastic modulus of river ice in compression at -3°C decreases with increase of stress.

Table 3: Elastic modulus of ice at different stress rates.

Stress, N/mm^2	0.105 – 0.368	0.368 – 0.632	1.157 – 1.420	1.168 – 1.946
Elastic modulus, N/mm^2	3,677	1,343	588	333

The elastic modulus of ice is, according to V. P. Berdennikov [16], a function of the ice temperature and decreases as the temperature increases. The temperature dependence increases with the salinity of ice and is a function of the liquid content in form of brine cells. The elastic modulus increases with the number of loading when the loading and unloading is frequently repeated and the rate of increase of the modulus decreases as the number of loading increases. Nakaya [16] it shows the elastic modulus of ice of density 0.910 – 0.914 g/cm^3 to be 8,826 N/mm^2, while ice of density 0.90 g/cm^3 has an elastic modulus of 6,865 – 7,845 N/mm^2 and ice of density 0,70 g/cm^3 a modulus of 3,923 N/mm^2. This show how the elastic modulus of ice depends on the density of the ice. The shear modulus characterizes the resistance of ice to shearing strain and expressed by the formula

$$G = \tau\gamma$$

where G [N/mm^2] is the shear modulus, τ [N/mm^2] is the tangential stress and γ [rad] is the angular strain. Same as with the elastic modulus, shear modulus faces same, or similar, challenges which causes discrepancies in the values obtained. American Meteorological Society [16] used the recommended values of the elastic modulus which to give shear modulus of ice accepted values

a) for calculating the elastic deformation during dynamic loading, $G \approx 2{,}942 - 3{,}334$ N/mm^2
b) for calculating the initial deformation during prolonged loading, $G \approx 1{,}471$ N/mm^2

Poisson's ratio is the coefficient of transverse deformation. When a sample is applied with compressive or tensile forces, the sample has a ratio of the transverse deformation to the longitudinal deformation, and the dimension of the sample may change freely in transverse direction. Poisson's ratio in association with the elastic modulus and shear moduli when elastic deformation occurs, is represented by following relation

$$\mu = \frac{E}{2G} - 1$$

where E [N/mm^2] is the elasticity module. From analysis by Veinberg [16], the results of the measurements of Poisson's ratio of ice, comparisons of the propagation velocities of longitudinal and transverse vibrations in ice, and comparisons of the elastic and shear modulus

from various researches, it was established that the value of the Poisson's ratio closest to reality is $\mu = 0.36 \pm 0.13$. B. D. Kartashkin [16] considered that an average Poisson's ratio is 0.34 for ice with temperature between $-5°C$ and $-16°C$. This was based on experimental determinations of the value of the elastic and shear moduli. However, B. A Savel'ev [16] recommended that in calculations the Poisson's ratio should be 0.36.

Key factor of ice mechanics is the microstructure which vary and depends mostly on conditions of formation as well as thermal and deformation history. There exist numerous different classification for ice microstructure, but to simplify the microstructures, it can be classified as

- Macrocrystalline ice which consists of large crystals and is oriented in vertical direction, thus having vertical C-axis (axes of symmetry) of individual crystals.
- Columnar ice which consists of columnar-textural with horizontal C-axis.
- Gramular ice which consists of crystals with roughly equal dimensions and generally having randomly-oriented C-axis, though some degree of alignment is possible.

Both macrocrystalline and columnar ice have ansitropical properties while granular ice has isotropical properties. Anistropical property is the property of being directionally dependent, which implies different properties in different directions, as opposed to isotropy which means uniformity in all orientations. To understand the mechanical property of ice formed on wind turbine blades, it is necessary to investigate formation and growth of atmospheric ice.

Atmospheric ice is porous as the microstructure consists of small grains with air bubbles trapped between the grain boundaries. The air bubbles will function as points of stress concentrations. Also, the pore pressure is generated entirely on volumetric strain and causes the poroelastic behavior of ice. This is done under the influence of loading conditions and the elastic compliance and stiffness tensor of porous ice which depends on porosity by volumetric strain and equivalent elastic pressure. Parameters such as growth conditions, air temperature, air velocity, median volume diameter of droplets and liquid water content of the air, as well as surface temperature of deposit, has an impact on the result of the formation of microstructure in atmospheric icing.

It was observed, during a study of ice structure, that there were no initial water film on the surface for wet growth regime. Instead, the large impacting droplets grew due to coalescing with other large and small droplets. However, it was observed that the droplets had a maximum size that could stay on an airfoil. If this size was surpassed, the aerodynamic forces acting on the droplet would overcome the adhesive forces and shed from the airfoil. The droplets acts as

a nucleation site where layers of ice forms and water film flow starts. This area dictates the growth process of ice, while gradual freezing surface water to ice layers. When the water flow stops, the growth process is uniform and all droplets freezes on impact. In a wet growth regime for wind turbines, the microstructure of the icing will vary over the length of the blade. This is due to the linear speed differences from root to tip of the blade. The density of accreted ice is governed by the Macklin parameter [8]

$$R = \frac{(-v_0)d_m}{2t_s}$$

When the density of the accreted ice decreases, the mechanical strength of the atmospheric ice tend to decrease as well. In the Macklin parameter, $-v_0$ [m/s] represent the droplets impact velocity, d_m [μm] is the diameter of droplets and t_s [°C] is the surface temperature. The Macklin parameter governs accreted ice density as follows

$$\begin{cases} \rho = 0.11R^{0.76} & for\ R \leq 10 \\ \rho = R(R + 5.61)^{-1} & for\ 10 < R \leq 60 \\ \rho = 0.92 & for\ R > 60 \end{cases}$$

This implies that accreted layers on a wind turbine blade becomes progressively mechanically weaker [8].

2.4. Adhesive properties of ice

Understanding adhesive affect ice has on different surfaces is a complex study. There are different variables to take into consideration such as angle of contact area for water to adhere to ice is different to different substances, imperfections distributed throughout the mass of ice and other solid substances, plastic-elastic properties of the involved substances, the adsorption of gases at the interfaces, solubilities in each other of the substances involved and surface roughness even down to molecular dimensions.

Jellynek [17] studied adhesive properties of ice and was done with the respect to stainless steel, polystyrene and polymethylmethacrylate (PMMA). It was based on cross-sectional area, thickness of the ice and the temperature and experiment were performed by applying forces in shear and in tension.

From experiments with shear force, where snow-ice was sandwiched between two stainless steel plates, three characteristics on adhesive strength were found: It is independent on cross-

sectional area, it is independent of the thickness of the ice layer and it is a linear function of temperature. The third discovery is true until the temperature becomes larger than the cohesive strength of ice at about $-13°C$. The adhesive strength found by the experiment showed, at the temperature of $-5.15°C$, that it was about 0.588 N/mm^2 in shear. In tension, if the disc was thin enough, it was 6,865 N/mm^2 and could have a larger stress at an even thinner disc without experiencing adhesive break. By using the Weibull distribution, which is expressed as

$$S_A = k_1 A^{-1/\beta} + C$$

the adhesive strength at the weakest imperfection that causes adhesive rupture can be calculated. In the equation S_A is the average adhesive strength, k_1, β and C are constants and A [m^2] is the cross-sectional area of the specimen. Also, when adhesive rupture of ice happens in a consecutive sequence, the adhesive strength is independent of the cross-sectional area [17].

In the Icing Research Tunnel at the NASA Lewis Research Center, adhesive shear and peel tests were done. The test provided data on the mechanical properties of rime and ice under controlled conditions. The maximum adhesive strength reached 120 psi between impact ice and smooth metal and neoprene surfaces.

Parametric studies of adhesive shear strength revealed it was not affected by ice thickness, cloud on-cloud off conditions, the material substrate rotation or non-rotation of the shear specimen, or the slope of the window of the shear. Results of adhesive shear strength shows significant scatter. Though fracture characteristics of most materials shows scatter, for ice it is much greater and is important for deicers and ice shape determinations.

Between ice, and either metal or neoprene surfaces, the peel strength showed to be extremely low and varies between 175 to 875 N/m at higher than normal peel angles [18].

2.5. Ice Deformation

Deformation of ice can be elastically, plastically or by brittle fracture when forces are applied. The main characteristics are its plastic properties and virtually non-existent elastic properties. The moment a load is applied, the elastic deformation occurs followed with immediate start of plastic deformation. The elastic, reversible, deformation and the plastic, residual, deformation are generally the two components of the total deformation. Plastic deformation occurs only in presence of shear stresses, while elastic deformation and densification occurs under equal, hydrostatic compression on monolithic ice. Brittle fracture occurs when the applied stress

exceeds the ultimate strength of the ice, but it can also occur when the dynamic load increases, which is expected under turbine operation. Also, temperature is an influenced factor of mechanical properties. Ice, and its cohesion in lattice of crystals, becomes weaker and its plastic properties increases when temperature is around 0°C. For atmospheric ice there are three influential factors for deformation of polycrystalline ice, which also support the recrystallization mechanism of ice

- Elastic and plastic deformations of the individual crystals
- Displacement of crystals with respect to each other
- Destruction of the crystals

These are factors that supports the recrystallization mechanism in ice. This allows formation of new crystals and growth of existing ones at the expense of disintegrated and overstressed crystals. There are three simultaneous processes in ice; work hardening due to partial rearrangement and redistribution of stresses, work weakening due to destruction of the bonds, and increased strain and relaxation.

With the relaxation of ice, creep is involved as with any other material subjected to creep behavior. The creep behavior has three stages;

- Primary stage has initially high strain rates which decreases as the recrystallization process continues
- Secondary stage referred as “steady-state creep” and is characterized by constant strain rate under constant loading
- Tertiary stage, the strain increases with exponential rate and eventually fails

Ice creep happens when the individual crystals along the grain boundaries, which are relative of each other, are slipping. This is temperature depended, and is known as thermally active glide and by Harper-Dorn creep, which is dislocation movement.

The expected stress failure of ice that is accreted on the wind turbine blade is caused by bending. The most probable scenarios of stress failure of ice on wind turbine blades is the cleaving of ice at the point of maximum shear stresses and rupture of the point of maximum tensile stresses. Since it is not likely that the tensile stresses in bending will surpass the maximum strength in tension, the maximum strength in bending is higher than the maximum strength in tension [8].

2.6. Ice Failure

There are different properties that influence the ice breaking from the blade such as temperature, porosity, salinity, crystallography etc, varies from different regions. This makes an accurate prediction of ice load difficult. There are three regimes of ice failure; the ductile regime, the transitional regime and the brittle regime.

Ductile failure happens when ice is loaded with a relatively slow strain rate. This allows stresses from deformation to relax and grain boundaries can slide with respect to each other after crossing the yield point.

The brittle crushing happens when the strain rate is very large. There might be a small elastic deformation followed by crack propagation. From elastic deformation, which is due to the elastic response of the crystal lattice from applied stress, there is a sudden failure without the yielding process [19]. It is usually in the transitional and brittle domain that ice shedding occurs [8]. Ice crushing can be split into three categories; intermittent crushing, frequency lock-in and continuous brittle crushing. This is based on the speed range for development of ice force and structure response, and caused by ice-induced vibrations. Ice deformation and failure at high indentation velocities and low aspect ratios defines ice crushing. It is a combined result of ice pulverization, formation of spalls and flakes, and formation of radial cracks [20]. Example of intermittent crushing of ice happens at low ice speed. Ice builds up to, and then oscillates around, a value which exceeds a buckling limit and deforms until buckling failure occurs. Ice has a certain loading capacity followed with a drop of ice load. This happens in a cycle and creates a saw-tooth feature shown in the graph of Figure 3 and is defined as a quasi-static response.

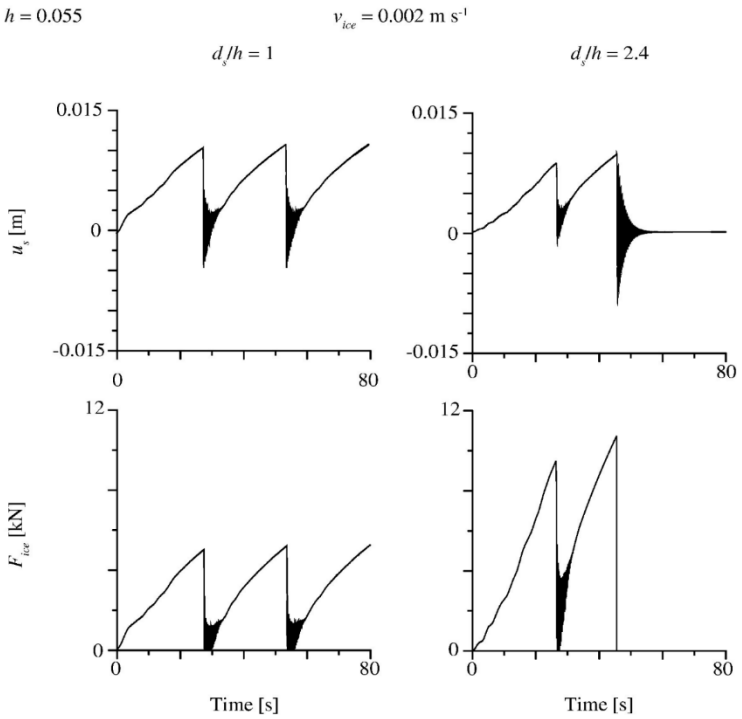

Figure 3: Example of intermittent crushing of ice [20].

The frequency lock-in phenomenon happens when the ice speed is between $0.06 - 0.10$ m/s and the crushing is continuous.

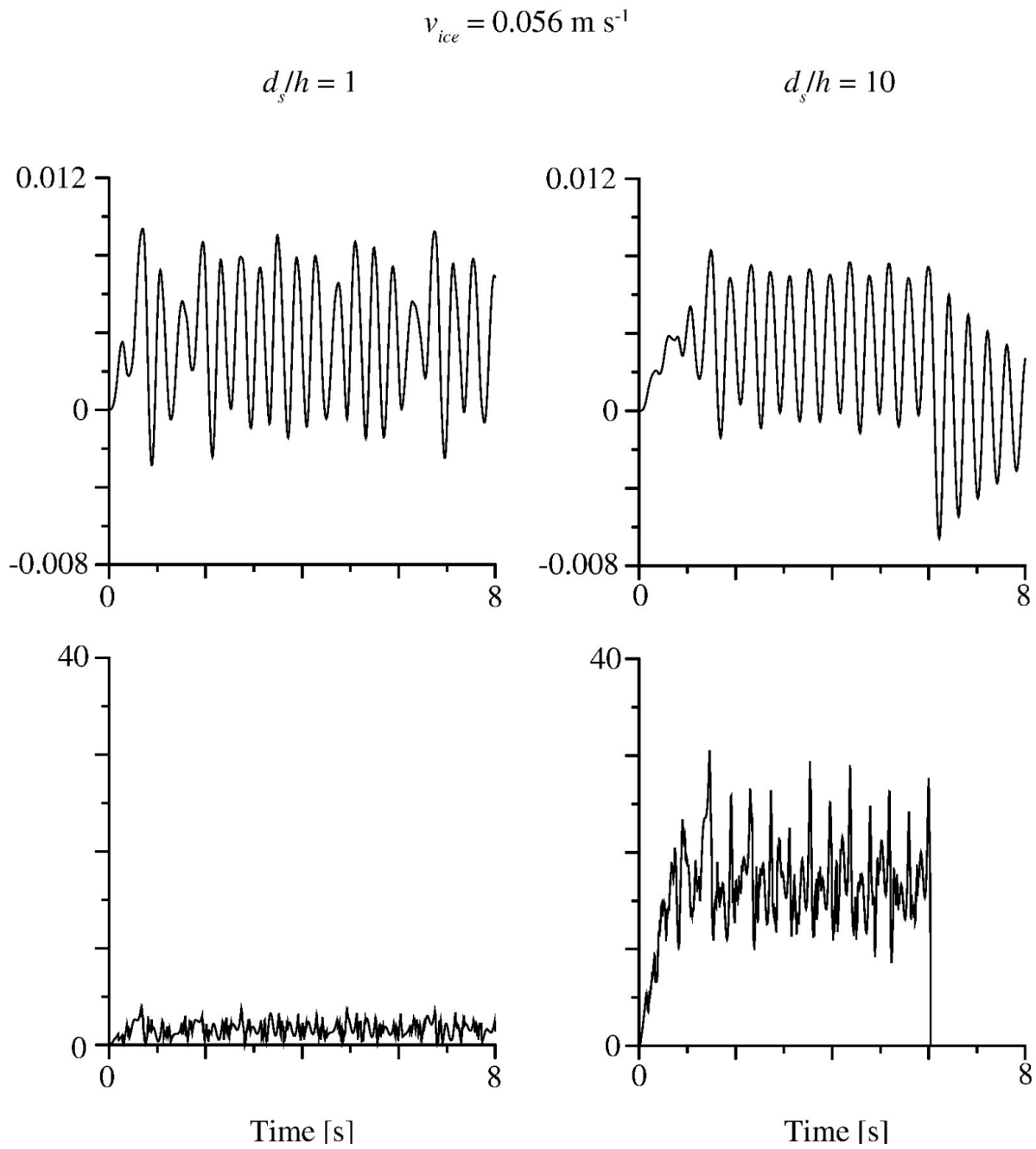

Figure 4: Example of frequency lock-in of ice [20]. Vertical axis for top two graphs is u_m[m] and the vertical axis for the bottom two pictures is F_{ice}[kN].

The continuous brittle crushing phenomenon happens when the ice speed is higher than 0.10 m/s. Between intermittent crushing and continuous brittle crushing, the frequency lock-in phenomenon may occur in which the natural frequency of the structure is within the ice loading frequency range and resonance might occur [19].

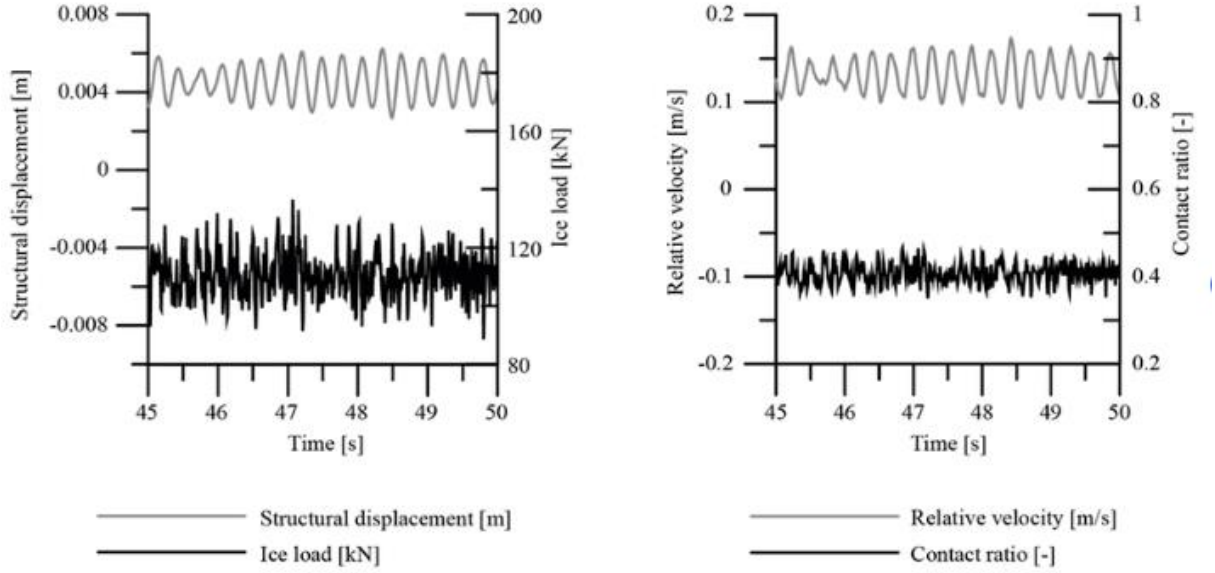

Figure 5: Example of continuous brittle crushing [40].

After certain intensity of strain rate, the atmospheric ice undergoes a ductile-to-brittle transition.

2.7. Accretion and ablation mechanism

To identifying icing event for a wind park atmospheric data used [21] to evaluate the icing model iceBlade, which process equation for both accretion and ablation mechanism.

The iceBlade model uses a simplified model of a wind turbine blade to approximate the mass of ice that accumulates during in-cloud icing conditions. Based on wind velocity on the rotational speed of the blade, the model can estimate the effect of liquid-phase cloud particles accreted.

The accretion model calculates the icing growth based on the flux of cloud particles and three correction factors (α_1, α_2 and α_3) which range from 0.0 to 1.0 the incoming mass flux. The correction factors represent the processes that reduce the amount of ice accretion from its maximum value. The efficiencies of these dimensionless factors are defined as collision (α_1), sticking(α_2) and accretion (α_3).

$$\frac{\partial M}{\partial t} = \alpha_1 \alpha_2 \alpha_3 \omega v A \tag{2.1}$$

The mass flux of cloud particles is a product of mass concentration of particles or liquid water content ω [g/m^3], the velocity v [m/s] and the cross-sectional area of the object A [m^2], and gives the change of mass M [kg] over change of time t [s].

The sticking efficiency is approximately unity of water droplets and wet snow under favorable conditions, and is equal to the reciprocal of true air speed for frozen droplets. The value of the accretion efficiency is depended on the growth regime of ice. For dry growth $\alpha_3 = 1.0$, but for wet growth the value is decided by the heat balance of the surface which is represented by

$$Q_f + Q_v = Q_c + Q_e + Q_l + Q_s$$

where Q_f [J] is the latent heat released during freezing, Q_v [J] is the frictional heating of air, Q_c [J] is the loss of sensible heat to the air, Q_e [J] is the heat lost due to evaporation, Q_l [J] is the heat loss in warming the impinging water to the freezing temperature and the Q_s [J] is the heat loss due to radiation. This equation is described in more details in ISO 12494. The surface thermodynamic model of the ice accretion process follows the so-called Messinger model. It is based on the temperature of an unheated surface in icing conditions. This works well for dry rime ice condition, but is more challenging when it comes to wet snow. The reason is that it neglects the surface water dynamics in the model, which result in inaccurate run back flow phenomena and heat conduction through the ice-water interface.

The icing model, equation (2.1), and the ISO 12494 model are not ideal for describing the icing process on wind turbines. They are more applicable for icing at low wind speed with objects of cylindrical shapes and overhead transmission lines. However, ISO 12494 defines a height factor

$$k = e^{0.01H}$$

where H [m] is height above terrain. This factor makes the models more suitable for wind turbines.

For more complicated enhanced physical models, software packages such as LEWICE, FENSAP-ICE, ICECREMO, CANICE, THERMICE, TRAJICE and TURBICE can be utilized. These models are not suitable for purely analytical modeling. These numerical models are computational fluid dynamic (CFD) simulations which are computationally demanding and

require a significant amount of computational power. Also, these models do not take into account of ice shedding, but only ice accretion process [8].

The ablation model refers to all processes that remove ice from a structure, and is categorized into three processes: melting, sublimation and shedding.

Melting and sublimation are physical process based on heat and moisture balance between the ice and the ambient air when the temperature is above and below the freezing point. Shedding occurs when ice falls from the structure due to loss of adhesion, and is split into partial shedding or total shedding. Partial shedding happens when ice loses cohesion with another part of the ice, and total shedding happens when ice lose adhesion to the structure. The following equation is used to calculate ice sublimation

$$\left(\frac{\partial m}{\partial t}\right) = \frac{4\pi r D f_v \rho_s(T_\infty)}{1 + \frac{L_s D f_v}{k f_h}\rho_s'}$$

where D [m^2/s] is diffusivity of water vapor in air, f_v [-] is the ventilation coefficient for water vapor,
$\rho_s(T_\infty)$ [g/m^3] is the saturation vapor density at ambient air temperature T_∞ [°C], L_s [J/g] is the latent heat of sublimation, k [$W \cdot m^{-1} \cdot K^{-1}$] is the thermal conductivity of air, f_h is the ventilation coefficient for heat, and ρ_s' is the derivative with the respect to $\rho_s'(T_\infty)$ [21].

3. Wind turbine blade

Today, Nordkraft Vind Narvik has a capacity of 32.2 MW with their 14 wind turbines placed at Nygårdsfjellet. The annual average production is 105 GWh, which is equal to the normal consumption of approximately 5,200 Norwegian households. At a wind speed of 3 m/s the production starts, and it is stopped at 25 m/s for safety reasons to prevent damages of the wind turbines. The average wind speed which is measured 50 m above the ground of the Norwegian coast is approximately 8 m/s [22].

Table 4: Technical data for wind turbines at Nygårdsfjellet, Narvik.

Technical data		
Tower height	80	m
Rotor diameter	90	m
Rotor area	6,361	m^2
Nacelle weight	82	tons
Tower weight	158	tons
Rotor weight	60	tons
Total weight	300	tons

3.1. Wind turbine blade material

A standard wind turbine blade has a length of 35 – 40 m for a 1.5 MW turbine, and weighs 6 to 7 tons. The aerodynamic design, which typically is composed of 70 – 75 % glass, must meet mechanical requirements of high rigidity and resistance to torsion and fatigue [23]. To achieve optimal properties for a wind turbine blade for increased efficiency, the following properties are evaluated; weight to reduce gravitational forces, strength to withstand wind forces and gravitational forces of the blade, fatigue resistance to withstand cyclic load and stiffness to ensure stability of optimal shape. The material properties should have; low density, long life and high performance, ease of processing, capability of recycling and reduced cost. The wind blade needs adequate stiffness, strength and extended fatigue resistance as well as optimal aerodynamic design.

To achieve these requirements, the material used is a composite material of fiber reinforced polymers of carbon, glass fibers and thermoset polymer. A composite material consists of two or more individual materials. The goal is to combine different preferred properties and to incorporate the best characteristics of each of the component material. Fiber glass is one of the most common composites where glass fibers are embedded within polymeric material. By combining glass fibers and polymeric materials the resulting material is relatively stiff, strong, flexible and ductile, and have a low density. The desired materials choice should also be eco-friendly and bio-degradable [24, 25].

The composite material dominating the wind turbine blade market is glass fiber-reinforced plastics (GRP) since it provides necessary properties at low cost. GRP has good mechanical properties, corrosion resistance, high temperature tolerance, ease of manufacture and favorable cost. Approximately 85% of all manufactured composite materials are GRP.

The physical form of reinforcements are significant factor for new material properties and is present in three different forms; particles, discontinuous and continuous fibers. Particles has a

spherical shape with approximately equal dimensions in every directions. Discontinuous fibers can have a length of a few millimeters to few centimeters, while the diameter most fibers does not exceed a few micrometers. Continuous fibers cause composite materials to manifest their anistropic functions [26]. When processed into the composite material, they are unidirectional and run longitudinally. The advantage of anistropic property is the ability to control the orientation of raw composite on the final structure, and important design criteria can be altered and customized. However, having effective fiber reinforcement in all three dimension is challenge and a disadvantage [27].

Glass fiber is manufactured by melting glass materials such as silicat, colemanit, aluminum oxide and soda. On wind turbine blades is E-Glass and S+R Glass types. E-Glass, or electrical grade glass, has excellent fiber forming capabilities and most used as the reinforcement phase in fiberglass. E-Glass has a tensile strength of 3,445 N/mm^2, a compressive strength of 1,080 N/mm^2, an elastic modulus of 73,000 N/mm^2 and density of 2.58 g/cm^3 [26], [27]. S-glass (Strength glass) on the other hand has a lower density of 2.49 g/cm^3, but higher tensile strength, 4,750 N/mm^2, and a higher elastic modulus at 89,000 N/mm^2. However, S-glass has a significant higher cost compared to E-glass, has a relatively low fatigue resistance and is self-abrasiveness if not treated appropriately which can reduce strength [28].

3.2. Forces acting on wind turbine blade

Either operational or idle, the wind turbine and its blades are subjected to many different forces. Important forces acting on the blade during operation are

- Aerodynamic
- Gravitational
- Centrifugal/Centripetal
- Gyroscopic
- Operational

Aerodynamic forces are caused by wind in form of a lift force, drag force and pitch moment. The drag force acts parallel to the direction of the fluid flow and will resist the motion of an object moving through a fluid like water and air. The amount of drag force is depending on the size and speed of the object relative to the difference of the air speed and the density of the air. Lift is force on a solid object that acts perpendicular to the flow of the fluid. It is created by the

pressure differences of variations in speed of the air at all points around the object. The air speed variations are caused by disruption and turning of the air flowing past the object. In aerodynamics the idea of air being classified as fluid is a principal concept. This is due to that behavior and flow of air, like all gasses, is in a similar matter as of a liquid. Another concept is the fact of lift, as well as drag, can only exist in the presence of a moving fluid [29].

Gravitational force is a force that attracts masses. In the case of gravitational force of the wind turbine blade, it is the force of the blades weight that is pulled by the Earth's force [30].

Centrifugal force and centripetal force comes from the inertia and rotation moment that acts on the blade. The difference between the two forces is the direction the force is acting. The centrifugal force is defined as "the apparent force, equal and opposite to the centripetal force, drawing a rotational body away from the center of rotation, caused by the inertia of the body". The definition of centripetal force is "The component of force acting on a body in curvilinear motion that is directed toward the center of curvature or axis of rotation". While centripetal force is an actual force, centrifugal force is an apparent force. An example of this is if a mass is attached to a string which is connected to a rotating center, the string exerts an inward force. However, the mass appear to exert an outward force on the string [31].

Gyroscopic force is based on the principal of angular momentum. A gyroscope rotates about an axis perpendicular to both torque and the angular momentum. This is due to the torque which is applied perpendicular to its axis of rotation and is also perpendicular to its angular momentum [32].

Operational forces are system dependent and are results of pitching, yawing, breaking and generator connection. Addition to the mentioned forces, there are also stochastic forces due to random variables such as gusts and wind shears [8].

4. Analytical analysis

To understand what stresses occur during ice cracking, analysis of simulations are done with different parameters. The two main directions in focus are forward/backward motion and up\down motion of the wind turbine blade. Before simulations, analytical and numerical analysis are carried out to give a theoretical understanding of bending and what forces that are acting on the blade.

The main four strains on the wind turbine blade are axial force N [N], shear force V [N], bending moment M [Nm] and torque τ [Nm]. Continuing with these strains and to understand their impacts on the wind turbine blade a model is drawn to illustrate the blade. Due to a generalization and simplification of a wind turbine blade, the blade is drawn in Inventor, however, without specific dimensions. It is a model just to give an idea for the results generated in Ansys, see Figure 6.

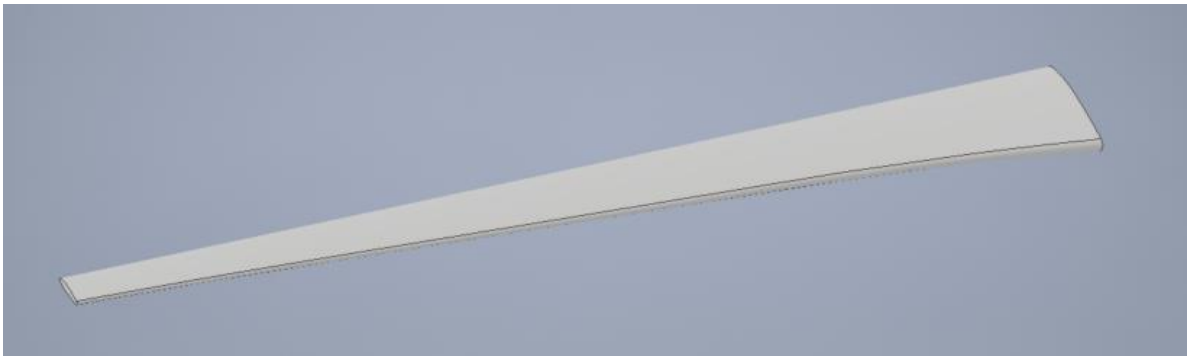

Figure 6: Model of a wind turbine blade drawn in Inventor.

4.1. Axial parallel shear force

Axial force, shear force, bending moment and torque represents the resultants of normal tension and shear stresses over a beam section. The axial force has an attack line through the cross section area center, while the torque is the resulting torque of shear stresses across the cross section. Due to the shear force V [N], the shear stresses over a beam section are normally small compared to the normal stresses due to the bending moment. Based on equilibrium considerations in the elementary beam theory, which decide cross section shear stresses with sufficient accuracy, axis parallel shear force can be calculated by calculating the shear force that is transferred into surfaces parallel with the beam axis. By considering a beam with variable bending moment $M(x)$ and constant shear force V [N], a formula can be derived for axis parallel shear forces. It also applies if the shear force varies.

Axis parallel shear force is noted as K [N] per unit length ∂x along the beam axis. The partial element has to be affected by a shear force parallel with the beam axis. The shear force $\overline{A}$ represented as $K \cdot \partial x$ and the equilibrium equation is then

$$K \cdot \partial x + \int_{A'} \sigma \, \partial A - \int_{A'} (\sigma + \partial \sigma) \, \partial A = 0 \tag{4.1}$$

where A' is a partial element of a sectional area. At this area the bending stresses σ [N/mm^2] and $\sigma + \partial\sigma$ [N/mm^2] acts in the direction of the beam axis. The bending stresses is formulated as

$$\sigma = \frac{M}{I}y, \qquad \sigma + \partial\sigma = \frac{M + \partial M}{I}y \tag{4.2}$$

where I [mm^4] is the moment of inertia and M [Nm] is the bending momentum.

With formula (4.2), formula (4.1) can be reduced to

$$K = \frac{1}{I}\frac{\partial M}{\partial x}\int_{A'} y\,\partial A$$

and since

$$\frac{\partial M}{\partial x} = V$$

the axial parallel shear force is

$$K = \frac{V}{I}\int_{A'} y\,\partial A$$

which again can be rewritten to

$$K = \frac{V}{I}S'$$

where S' is the integral of the static torque of the surface A' about an axis. To understand how the axial parallel shear force is distributed as shear stress over surface $\overline{A}$, a closer look at the sectional shear stresses will give a better understanding [33].

4.2. Sectional shear stresses

With a sectional plan $\overline{A}$ that is parallel with the neutral plan XZ, the assumption that the shear stress $\tau = \tau_{xy} = \tau_{yx}$ [N/m^2] is even distributed over the width b [m] of the sectional plan is a fairly accurate assumption. This is by reasoning: By elementary beam theory the beam will get the same bending stresses thus τ-distribution seen in Figure 7 if the beam was divided in n independent plates, with each of height h [m] and width b/n. The sectional shear stresses is represented by formula

$$\tau_{xy} = \frac{K}{b} = \frac{V}{Ib} S' \tag{4.3}$$

where the resultant of τ_{yx} [N/mm^2] over the beam cross section is equal to the shear force V [N]. As seen on Figure 6, the beam cross section can have a τ_{zx}-component and when the sectional shear stress τ [N/mm^2] near the surface is parallel with the contour of the cross sections, the beams surface is tension free according to Figure 7b.

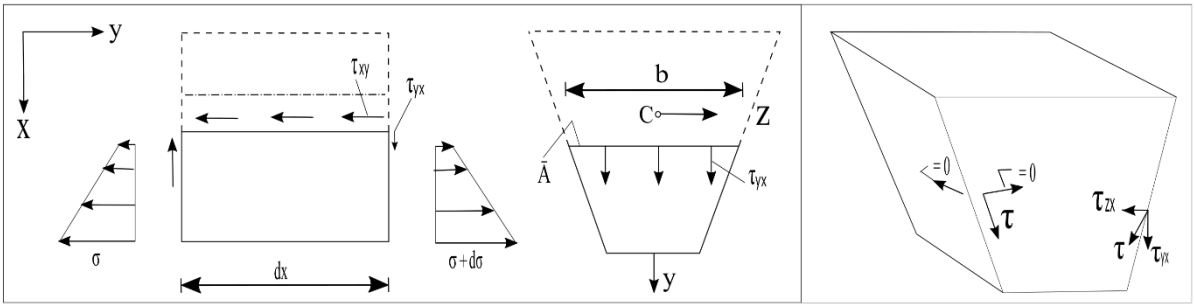

Figure 7: Sectional shear stress [33].

In Z-direction τ [N/mm^2] has the component τ_{zx} [N/mm^2] while having τ_{yx} [N/mm^2] in Y-direction.

From Figure 8, it is shown that the moment of area is greatest when the sectional area goes through the area center C [33].

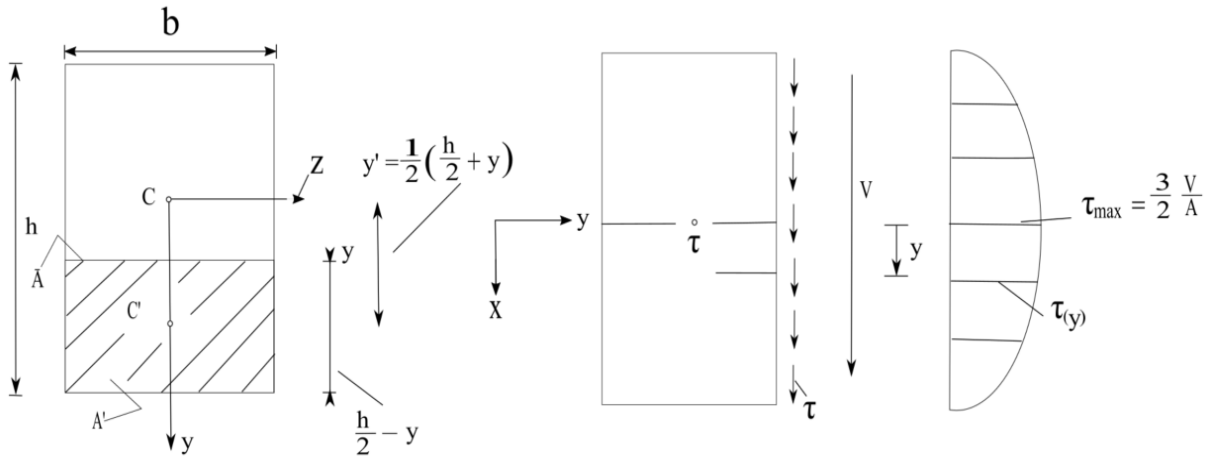

Figure 8: Shear stress distribution over a rectangular beam section [33].

4.3. Deformation of beams

The elastic line is the deflected beam axis and is expressed as deflection $u(x)$. With $u(x)$ the inclination angle $\emptyset(x)$ [rad] between the elastic line and X-axis can be calculated. From the elementary beam theory there are three hypotheses to derive bending stresses:

1. Deformation hypothesis, also known as Bernoulli's hypothesis, states that planar cross-section remains flat cross-section upon bending.
2. Stress hypothesis which states that normal stresses on planes parallel to the beam axis can be neglected.
3. Material hypothesis states that a material is linear elastic.

A fourth hypothesis for the elementary beam theory which builds on the following assumption

4. Deformation hypothesis II states that the deflection gradient $\partial u/\partial x$ is much less than 1. The hypothesis implies that the angular can be set as $\phi = \tan(\phi)$ [rad] due to the tangent to the slope ϕ [rad] is equal to $\partial u/\partial x$.

By the deformation hypothesis II the angular approximation is expressed as

$$\phi = \frac{\partial u}{\partial x} \ll 1 \tag{4.4}$$

Bases on the three first hypothesis deriving curvature gradient is expressed as

$$\kappa = \frac{1}{R} = \frac{M}{EI} \tag{4.5}$$

where κ is the curvature, EI is bending stiffness and R is the curvature gradient to the neutral surface of the beam. Due to the slope decreases the differential $\partial\phi$ is expressed negative

$$\partial\phi = -\frac{\partial s}{R} \Longrightarrow \frac{\partial\phi}{\partial s} = -\frac{1}{R}$$

where ∂s [m] is the element length. Combined with equation (4.4) results in

$$\frac{\partial\phi}{\partial s} = -\kappa = -\frac{1}{R} = -\frac{M}{EI} \tag{4.6}$$

and by deformation hypothesis II implies $\partial s = \partial x$ and the approximation of equation (4.3) gives

$$\frac{\partial^2 u}{\partial x^2} = -\frac{M}{EI} \tag{4.7}$$

Equation (4.7) is called the differential equation for the elastic line and is also known as Euler-Benoulli-equation. The equation can be applied if the bending stiffness EI varies with X, which is a function of the bending moment, given the variation is not to strong. Due to a number of partial loads which affects a beam simultaneous, equation (4.7) can be superimposed where the sum of the deflection is due to the sum of the partial load. When multiple loads works at the same time, the bending moment will be $M(x) = \sum_{i=1} M_i$ and deflection will be $u(x) = \sum_{i=1} u_i$.

Solving the equation with integration requires two boundary conditions, either by knowing the deflection or the slope of the beam ends. When the beam is loaded with a distributed load, $q(x)$ [N/m], the bending moment is decided alternatively by differential equations

$$\frac{\partial V}{\partial x} = -q(x), \qquad \frac{\partial M}{\partial x} = V(x) \Longrightarrow \frac{\partial^2 M}{\partial x^2} = -q(x)$$

Equation

$$\frac{\partial^2 M}{\partial x^2} = -q(x)$$

is called the beams differential equation and can be associated with the differential equation for the elastic line. This gives a 4. order differential equation, developed by Leonhard Euler, given the bending stiffness, EI, is constant [33],

$$\frac{\partial^4 u}{\partial x^4} = \frac{q(x)}{EI}$$

4.4. Curvature surface theorem

Discontinuous cross-sectional changes for a beam gives discontinuity in the curvature. Concentrated loads on a beam gives a buckling in the moment diagram. The curvature is then given by multiple functions for the buckling M/EI. This makes direct integration of equation (4.7) for deflection more complicated.

There are two method for deciding deflection of a straight beam. One method applies to all straight beams, while the other method applies to a beam which is freely supported between two endpoints. The methods are known as curvature surface methods and is based on the area of curvature diagram for

$$\kappa(x) = \frac{M}{EI}$$

To decide rotation angle θ [rad] for beam tangent at position B on the beam relative to the tangent at position A and displacement v, or tangent aside, of B relative to the beam tangent at A there are to formulas

$$\theta = \int_0^L \frac{M}{EI}\partial x$$

$$v = \int_0^L (L - x)\frac{M}{EI}\partial x$$

The two formulas gives following theorems [33]:

- First curvature surface theorem
  Rotation angle for the beam tangent at point B on the beam axis relative to the beam tangent on point A on the beam axis is equal to the curvature surface between the two points.
- Second curvature surface theorem
  Tangent aside v for point B on the beam axis relative to the beam tangent in point A on the beam axis is equal to the area moment around B of the curvature surface between the two points.

4.5. Unsymmetrical cross section

When a beam has an unsymmetrical cross section and is loaded in such way so the sectional forces over the cross section is axial force N [N], bending moments M_z [Nm] and M_y [Nm] and shear forces V_y [N] and V_z [N]. The sectional forces is resultants of normal tension σ [N/mm^2]

and shear tension τ [N/mm^2] over the beam section. The beam axis is represented with X-axis going through the cross-sectional area center.

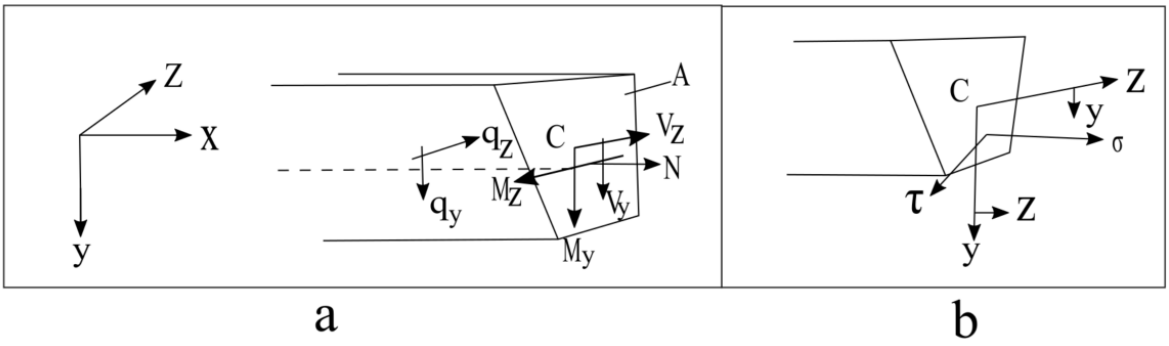

Figure 9: a) shows the beam with sectional forces over the beam cross section and b) shows normal tension σ [N/mm2] and shear tension τ [N/mm2] over the beam cross section.

The axial force is positive as tensile force and is perpendicular to the cross section and acts through the area center and is expressed as

$$N = \int_A \sigma \, \partial A \tag{4.8}$$

The bending moments are expressed by

$$M_z = \int_A \sigma y \, \partial A, \qquad M_y = \int_A \sigma z \, \partial A \tag{4.9}$$

Shear forces V_y [N] and V_z [N] is resultants of shear tension τ [N/mm^2] over and acts in the cross section. Shear force V_y [N] does not, in general, have an attack line going through the area center C without the cross section transferring a torsion momentum if XY-plane is not a symmetry plane. The same goes for XZ-plane and V_z [N].

By equilibrium considerations these relationships can be derived

$$\frac{\partial V_y}{\partial x} = -q_y, \qquad \frac{\partial V_z}{\partial x} = -q_z \tag{4.10}$$

$$\frac{\partial M_z}{\partial x} = V_y, \qquad \frac{\partial M_y}{\partial x} = V_z \tag{4.11}$$

This presents the elementary beam theory for beams with arbitrary cross section and gives four hypothesis given in section 4.3 “Deformation of Beams”. The three first hypothesis gives the formula for normal tension over a beam section, while the fourth hypothesis is necessary to get a theory to calculate beam deflections.

Bernoulli's hypothesis implies that the beam element with length ∂x [m] deforms as Figure 10 shows.

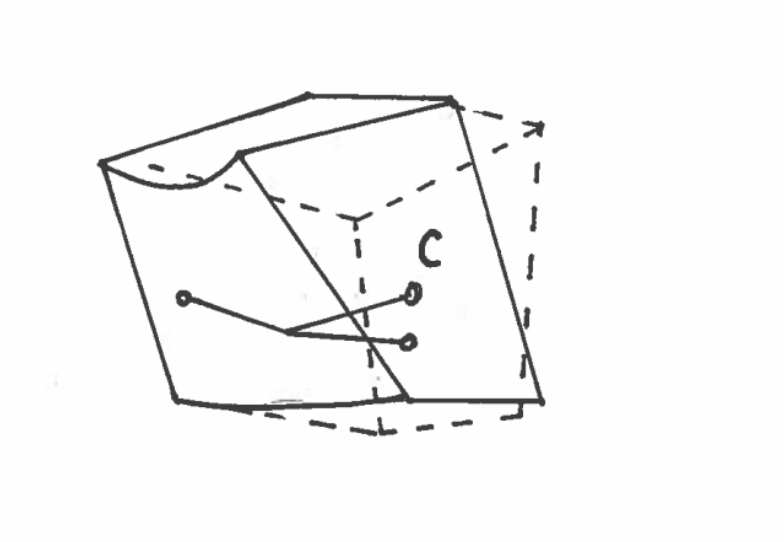

Figure 10: Deformation of beam element ∂x.

The figure shows that the strain parallel with the beam axis varies linearly with the coordinates y and z which gives equation

$$\varepsilon(x, y) = \varepsilon_0 + \kappa_y y + \kappa_z z \tag{4.12}$$

where coefficients ε_0 [-] , κ_y [-] and κ_z [-] is functions of x. ε_0 [-] corresponds to a relative parallel displacement of two cross sectional areas to the beam element. $\kappa_y y$ and $\kappa_z z$ represents the bending in XY-plane and XZ-plane where the coefficients κ_y [-] and κ_z [-] is the beams curvature in those two planes.

Normal stress distribution over a beam section is given by the strain equation (4.12) along with stress hypothesis and material hypothesis expressed as

$$\sigma = E\varepsilon = E\varepsilon_0 + E\kappa_y y + E\kappa_z Z \tag{4.13}$$

This expression together with equation (4.8) and (4.9) for tension resultants gives

$$N = \int_A \sigma \, \partial A = E\varepsilon_0 \int_A \partial \, A + E\kappa_y \int_A y \, \partial A + E\kappa_z \int_A z \, \partial A \tag{4.14}$$

$$M_z = E\varepsilon_0 \int_A y \, \partial A + E\kappa_y \int_A y^2 \, \partial A + E\kappa_z \int_A yz \, \partial A \tag{4.15}$$

$$M_y = E\varepsilon_0 \int_A z\,\partial A + E\kappa_y \int_A zy\,\partial A + E\kappa_z \int_A z^2\,\partial A \tag{4,16}$$

Equation (4.14), (4.15) and (4.16) can be reduced to

$$N = E\varepsilon_0 A \tag{4.17}$$

$$M_z = EI_z\kappa_y + EI_{yz}\kappa_z \tag{4.18}$$

$$M_y = EI_{yz}\kappa_y + EI_y\kappa_z \tag{4.19}$$

by using cross section constants

$$I_z = \int_A y^2\,\partial A - \text{Inertia of Z-axis}$$

$$I_y = \int_A z^2\,\partial A - \text{Inertia of Y-axis}$$

$$I_{yz} = I_{zy} = \int_A zy\,\partial A - \text{Centrifugal moment with regards of YZ-axis}$$

Equation (4.17), (4.18) and (4.19) is solved with regards of ε_0 [-], κ_y[-] and κ_z [-] and is expressed as

$$\varepsilon_0 = \frac{N}{EA} \tag{4.20}$$

$$\kappa_y = \frac{I_y M_z - I_{yz} M_y}{E\left[I_y I_z - \left(I_{yz}\right)^2\right]} - \text{Curvature in XY-plane} \tag{4.21}$$

$$\kappa_z = \frac{I_z M_y - I_{yz} M_z}{E\left[I_y I_z - \left(I_{yz}\right)^2\right]} - \text{Curvature in XZ-plane} \tag{4.22}$$

By using equation (4.17) the equation for normal tension over a beam cross section, also known as Naviers equation, can be derived

$$\sigma = \frac{N}{A} + \frac{yI_y - zI_{yz}}{I_y I_z - \left(I_{yz}\right)^2} M_z + \frac{zI_z - yI_{yz}}{I_y I_z - \left(I_{yz}\right)^2} M_y \tag{4.23}$$

By Deformation hypothesis II of small angles of inclination for the beam tangent implies that curvature κ_y in

XY-plane and κ_z in XZ-plane can be expressed as

$$\kappa_y = -\frac{\partial^2 u_y}{\partial x^2}, \qquad \kappa_z = -\frac{\partial^2 u_z}{\partial x^2} \tag{4.24}$$

Here, buckling in Y-direction is termed u_y and buckling in Z-direction is termed u_z. By implementing terms for Y- and Z-direction into equation (4.21) and (4.22) gives

$$\frac{\partial^2 u_y}{\partial x^2} = -\frac{I_y M_z - I_{yz} M_y}{E\left[I_y I_z - \left(I_{yz}\right)^2\right]} \tag{4.25}$$

$$\frac{\partial^2 u_z}{\partial x^2} = -\frac{I_z M_y - I_{yz} M_z}{E\left[I_y I_z - \left(I_{yz}\right)^2\right]} \tag{4.26}$$

and when YZ is a principal axis of the cross for the cross section so $I_{yz} = 0$ equation (4.25) and (4.26) reduces to

$$\frac{\partial^2 u_y}{\partial x^2} = -\frac{M_z}{E I_z}, \qquad \frac{\partial^2 u_z}{\partial x^2} = -\frac{M_y}{E I_y}$$

Deflection of a beam normally happens of the beams' plane normal to the neutral axis given that the placement of the neutral axis does not change along the beam axis.

By using known solutions from symmetrical beams the deflection and inclinations for unsymmetrical beams can be decided. Starting with calculating the equivalent inertia moment I_e [mm^4] given as

$$I_e = I_z - \frac{\left(I_{yz}\right)^2}{I_y} \left(\text{for } u_y \text{ and } M_z\right)$$

Here the inertia moment is of the Z-axis for the unsymmetrical beam and the deflection happens in Y-direction so the function is $u_y(x)$ of the deflection function $u(x)$. By assumption of knowing deflection function $u(x)$ for a beam which is symmetrical of XY-plane and has its stock conditions in this plane with the bending moment M_z [Nm] for the unsymmetrical beam calculation can be done.

Using equation (4.25) and bending moment M_z [Nm] gives the curvature

$$\kappa = -\frac{\partial^2 u}{\partial x^2} = \frac{M_z}{EI}, \qquad \kappa_y = -\frac{\partial^2 u_y}{\partial x^2} = \frac{M_z}{I_e}$$

This states that the relationship between the curvatures is constant along the beams axis

$$\frac{\kappa_y}{\kappa} = \frac{I}{I_e}$$

due to the stock boundaries is the same in XY-plane gives

$$u_y(x) = \frac{I}{I_e} u(x) \tag{4.27}$$

Deflection $u_y(x)$ is an expression of the unsymmetrical beam based on bending moment M_z [Nm] and by presumably know $u(x)$.

Same goes for equation (4.27) and by using bending moment M_y [Nm] under the presumption

1. $u(x)$ is the deflection in xy-plane for the symmetrical beam due to bending moment $M = M_y$ [Nm] around Z-axis.
2. The equivalent inertia moment is set as equal to

$$I_e = I_{yz} - \frac{I_y I_z}{I_{yz}} \left(\text{for } u_y \text{ and } M_y\right)$$

For deflection $u_z(x)$ in Z-direction the equation is set as

$$u_z(x) = \frac{I}{I_e} u(x)$$

where $u(x)$ is the deflection in Z-direction of a beam that is symmetrical about the XZ-plane and have the same stock conditions in XZ-plane as the unsymmetrical beam. This gives the equivalent inertia moment I_e [mm^4] [33]

$$I_e = I_{yz} - \frac{I_y I_z}{I_{yz}} \left(\text{for } u_z \text{ and } M_z\right)$$

$$I_e = I_y \frac{\left(I_{yz}\right)^2}{I_z} \left(\text{for } u_z \text{ and } M_y\right)$$

5. Numerical analysis

For the numerical analysis, a model is made in Inventor as a CAD-file, computer aided design, as mentioned in section regarding analytical analysis. Inventor is a parametric software used to model 3D mechanical design, design communication, tooling creation and product simulation. The user can input driving loads, dynamic components, friction loads to integrate motion

simulation and assembly. This gives the user the ability to run dynamical simulation to test the modelled product function in a real-world scenario by finite element analysis (FEA) [34].

For simulation the CAD-file is used for the finite element method (FEM) in Ansys. Ansys is a FEA tool that performs structural, thermal and electromagnetic analyses [35]. FEM is a numerical technique that uses partial differential equations to understand and quantify structural and fluid behavior, thermal transport, wave propagation and growth of biological cells [36].

5.1. Method for creating the wind turbine blade

To create the model in Inventor X and Y-coordinates where plotted in Excel, found in Appendix A, and inputted by using "Points" under "Insert" category for "2D Sketch" mode. Six additional work planes are added for sketching the wind turbine blade profile. The distance for each work plane are based on the distance from the original work plane (OWP), given in Table 5.

Table 5: Work plane distance in Inventor.

Work Plane	Distance from OWP [mm]
OWP	0.000
WP1	2,924.340
WP2	6,057.490
WP3	12,323.797
WP4	18,590.104
WP5	24,856.411
WP6	27,989.561

For each work plane a sketch is made for drawing the wind turbine blade profile for selected area. The profiles are based on the original profile (OP), given in Table 6.

Table 6: Profile sizes compared to original profile for sketches.

Profile	Percentage of OP [%]
OP	1.000
P1	0.861
P2	0.756
P3	0.621
P4	0.485
P5	0.358
P6	0.313

When all sketches are drawn, the Loft-function is used by selecting the sketches to create a solid, 3D model. The CAD-file is then exported as a IGEN- or STEP-file.

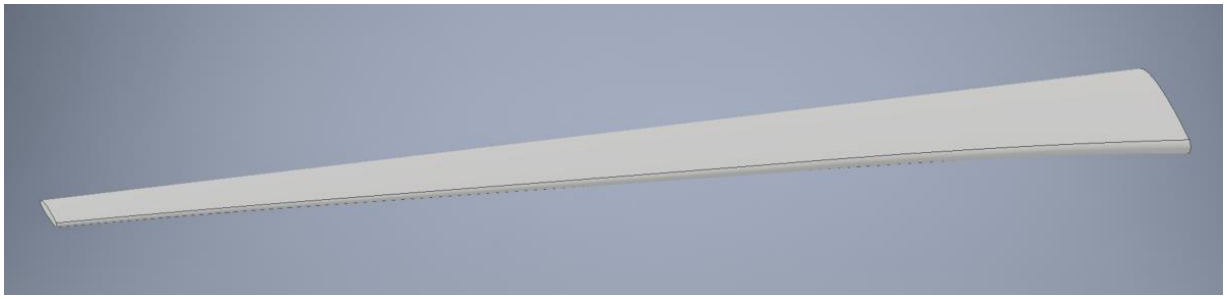

Figure 11: Wind turbine blade made in Inventor.

5.2. Method for fluent flow analysis

To be able to do a static structural analysis, a computational fluid dynamic analysis was done to obtain the forces affecting the wind turbine blade from the wind velocity. The geometry was imported for fluent flow (fluent) analysis in Ansys, and then edited in DesignModeler. In DesignModeler the model was enclosed by Enclosure-function so it could be assigned a fluid for the analysis. Then Boolean-function was added so the geometry of the wind turbine blade is subtracted from the geometry of the Enclosure-function, which later will be assigned air as the fluid surrounding the wind turbine blade.

After Boolean-function was added, the work in DesignModeler was done. Next step was the meshing. The mesh used had a quality of target skewness set to default, which is 0.9, and a medium smoothening. For the model there where 18,783 nodes and 105,842 elements. A node is a coordinate location in space where the degrees of freedom (DOF) are defined. The DOFs represent the possible movement of this point due to the loading of the structure. Also, DOFs represents which forces and moments are transferred from one element to the next by mathematical relation. An element is the basic building block of FEA. The object modeled for FEA, and what type of analysis is being performed, determine what type of element is used [37]. More details are listed in Appendix B. When meshing the model inlet and outlet for the velocity is selected.

The final input for the analysis was then edited in Setup for Fluid Flow in Ansys. In the setup the model is set to k-epsilon (2 egn) for “Viscous – Laminar” under “Solution Setup” and “Model”. Next is input the velocity of wind, which is done under “Boundary Conditions”. The velocity used for the analysis is 10 m/s. Under “Solution Methods”, both “Turbulent Kinetic Energy” and “Turbulent Dissipation Rate” is set to second order upward. The analysis is done with 300 iterations, which is inputted in under “Run Calculation”. To see the results for forces in X, Y and Z-directions, wall-surroundings is selected for “Results” and “Contours”.

5.3. Results from fluid flow analysis

Table 7: Results in absolute value from Fluid Flow analysis.

Velocity: 10 m/s	**Force [N]**
X	218
Y	76
Z	92
Velocity: 25 m/s	
X	1,356
Y	476
Z	580

5.4. Method for static structural analysis

After Ansys Workbench is opened, static structural, under analysis system, is selected. Before doing an analysis the material is selected in "Engineering Data". The material selected is E-Glass due to it being widely used for wind turbine blades. After material selection the IGEN- or STEP-file, exported from Inventor for the wind turbine blade, is imported and the model is meshed. The model is meshed with 1,720 nodes and 300 elements. More details is in Appendix C. When the model is meshed, input for the static structural is added with standard earth gravity on the wind turbine blade, rotational velocity, fixed support and an evenly distributed force.

The analysis is executed four times with forces for 10 m/s, and four times with forces for 25 m/s, as given in Table 7. For the wind velocities the analysis are done in $\pm$ Y-direction and $\pm$ Z-direction, which represents when the blade is in 0°, 90°, 180° and 270° position of the rotation of the wind turbine blade.

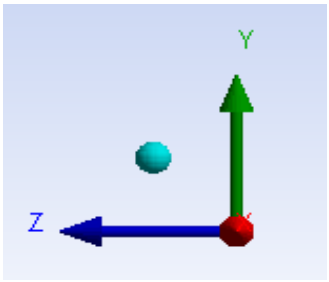

Figure 12: Y- and Z-axis.

For all of the analysis the rotational velocity is placed at the mid-section on the wind turbine blade, as seen in Figure 12. The velocity is set to -12 rpm in X-direction and 12 rpm in Z-direction, which tilts the blade at an angle of 45°.

5.5. Results from structural analysis

The first analysis the standard earth gravity is set in +Y-direction and the force input is for 10 m/s in X-, Y- and Z-direction as given in Table 6.

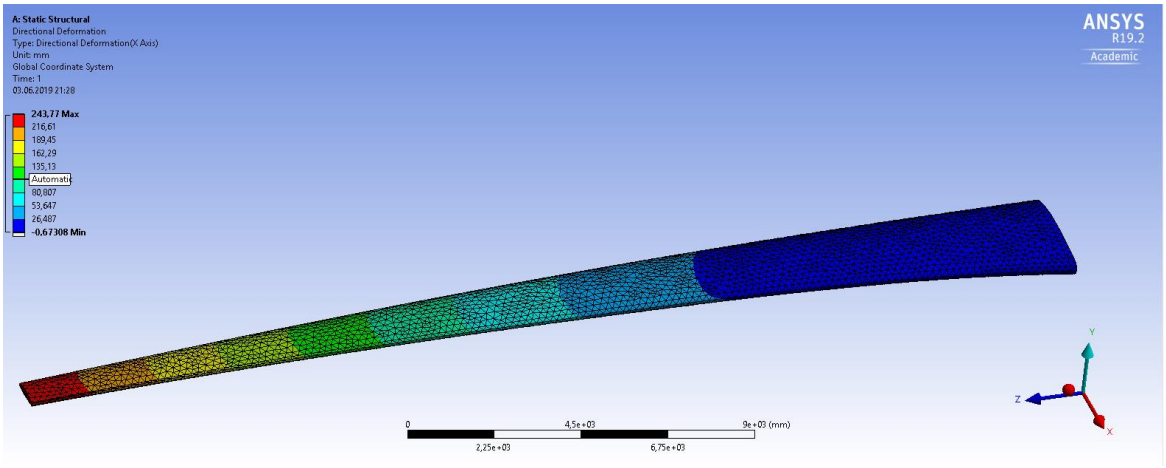

Figure 13: Directional deformation for the blade in +Y-direction at 10 m/s.

The blade's maximum deflection is at 0.244 m.

Analysis when the standard earth gravity is set in –Z-direction and the wind turbine blade is at 90°.

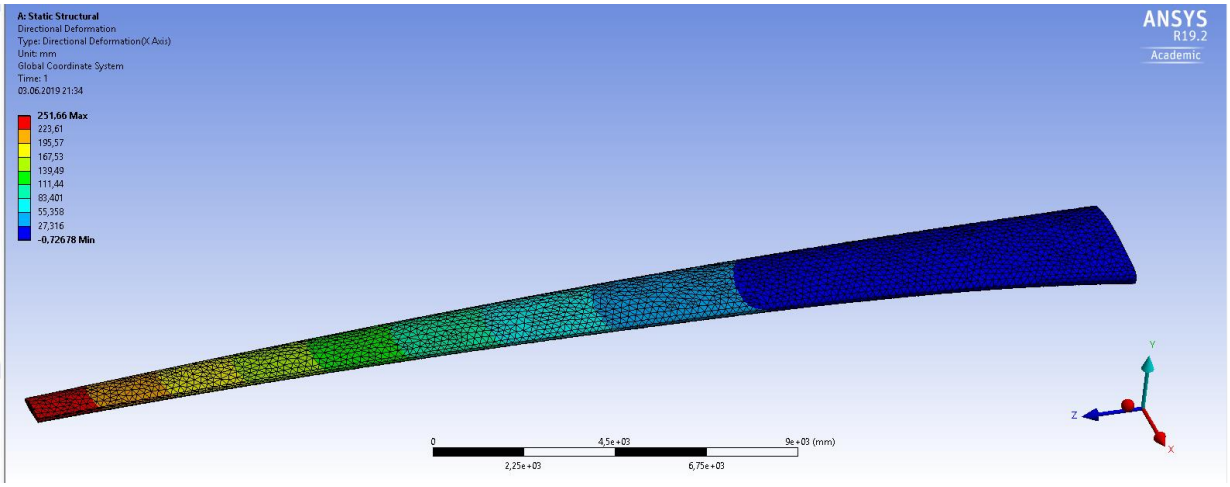

Figure 14: Directional deformation for the blade in -Z-direction at 10 m/s.

The blade's maximum deflection is at 0.252 m.

Analysis when the standard earth gravity is set in –Y-direction and the wind turbine blade is at 180°.

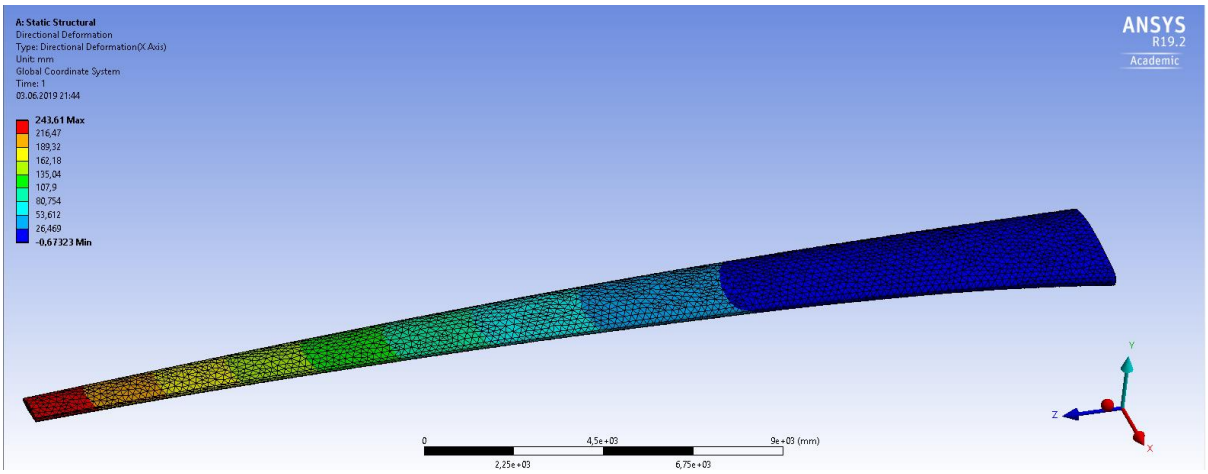

Figure 15: Directional deformation for the blade in +Y-direction at 10 m/s.

The blade's maximum deflection is at 0.243 m.

Analysis when the standard earth gravity is set in +Z-direction and wind turbine blade is at 270°.

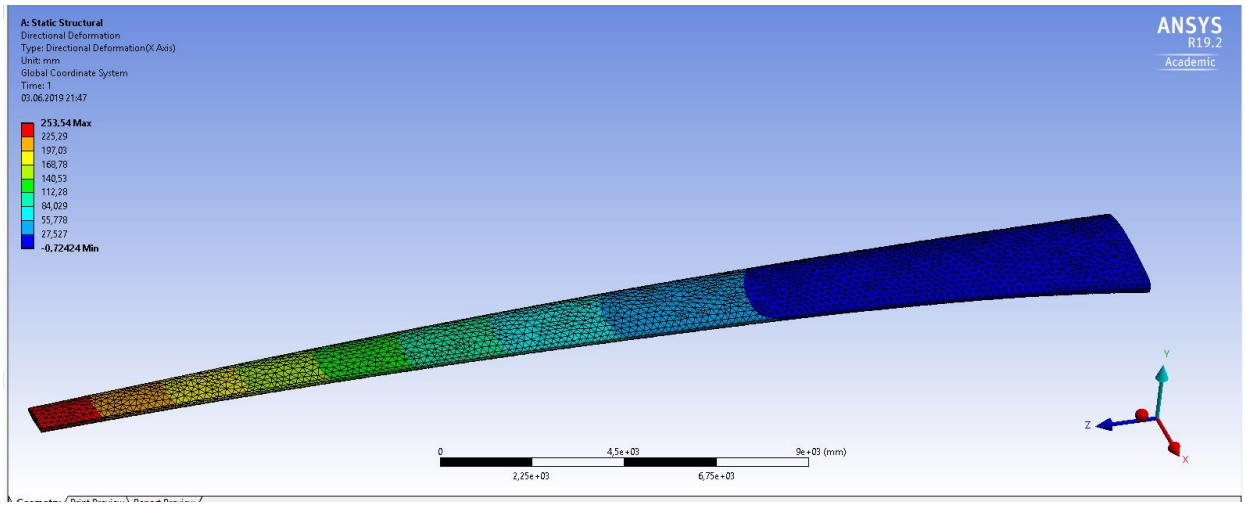

Figure 16: Directional deformation for the blade in +Z-direction at 10 m/s.

The blade's maximum deflection is at 0.254 m.

For all analysis the number of elements are 31,489, the number of nodes are 45,960 and the elements are SOLID187 and SURF154. These selections are done automatically by Ansys. SOLID187 is defined by 10 nodes having three degrees of freedom at each node and the element has plasticity, hyperelsticity, creep, stress stiffening, large deflection, and large strain capabilities. It is well suited to model irregular meshes and has a quadratic displacement behavior [38]. SURF154 is used for various load and surface effect application in 3D structural analysis [39].

Table 8: Results from ansys analysis for 10 m/s and 25 m/s.

Direction	Wind turbine blade position	Results: 10 m/s	Results: 25 m/s
-Y	0°	0.244 m	0.262 m
-Z	90°	0.254 m	0.252 m
+Y	180°	0.243 m	0.244 m
+Z	270°	0.254 m	0.254 m

Another analysis was executed where the rotation velocity was set to 12 RPM around the X-axis, and a load of 100,000 N was used. Reason for this is to see how it affects the deflection of the blade given the results in Table 8 is not as expected.

Table 9: Direction deformation of the blade when the load is set to 100,000 N.

Direction	Wind turbine blade position	Results: 10 m/s
-Y	0°	0.267 m
-Z	90°	0.257 m
+Y	180°	0.250 m
+Z	270°	0.259 m

5.6. Results from previous work

From previous work [8] similar analysis has been done for analyzing ice shedding from a wind turbine blade. In this work, the analysis has been done with the help of Ansys, MATLAB and MuCAD. MATLAB js numerical computing environment and MuPAD is a computer algebraic system (CAS).

The parameter used for this analysis are listed in Table 10.

Table 10: Turbine operation parameter from previous work [8].

Parameter	Value
Blade rotational velocity	15 RPM
Inflow wind speed	15 ms^{-1}
Air density	1.2922 kgm^{-3}
Lift/drag ratio	30

These values was chosen to match operation conditions for SWT-2.3-93 wind turbines. The material choice was S-glass fiber. The model had a homogeneous, solid, uniform cross-sections. The model, as with this thesis model, was tested with rotation position of the wind turbine blade at 0°, 90°, 180° and 270°. Ansys's chosen element was SOLID185, which is defined by eight nodes having three degrees of freedom at each node. The element has the same capabilities as SOLID187. The analysis, also same with this thesis, focused mainly in deflection of the wind turbine blade. For obtaining analytical and numerically results MuPAD was used and compared with the Ansys results. By testing, the desired results was produced by using Young's modulus of 40,000 N/mm^2, which gave the results listed in Table 11.

Table 11: Deflection of beam with Young's modulus at 40,000 N/mm^2 [8].

θ	Ansys [m]	MuPAD [m]
0°	1.728	1.980
90°	1.255	1.403
180°	1.729	1.980
270°	2.202	2.557

The bending of the blade during operation may not be the mechanism for ice failure, but a precursor to it. There are two possible states to consider for ice shedding, which are:

- Ice is in ductile state
- Ice is in brittle state

According to Kermani, Eskandarian and Cole [8], the most important mechanical property of ice when it is in a ductile state with low strain rate is the viscoelastic properties. The viscoelastic properties control the creep behavior of ice, as well as viscous strain effects. Creep-accumulated strains will cause ice to eventually fail as seen from experimental work of Mellor and Cole [8]. In brittle state, cracking of ice will cause it to rupture and fail. Indicated by Voitkovskii [8], small additional loading at higher load rates under cycling loading can cause premature rupture of ice. Important crack propagation for wind turbine blades is random stochastic loadings such as wind gust. Also, blade vibrations and vibrations induced by unbalanced loading of accumulated ice may affect ice deformation.

By ice throw date by Catting and Hutton [8] a consistent peak of deflection, stresses and strains at blade position 270°, the throw frequency is at maximum within of the vicinity of this blade position. This is due to the deflection change of the wind turbine blade during rotation, which over time will cause rupture and failure from cracks occurring during operation that loses adhesion with the blade surface.

5.7. Comparison between thesis and previous work

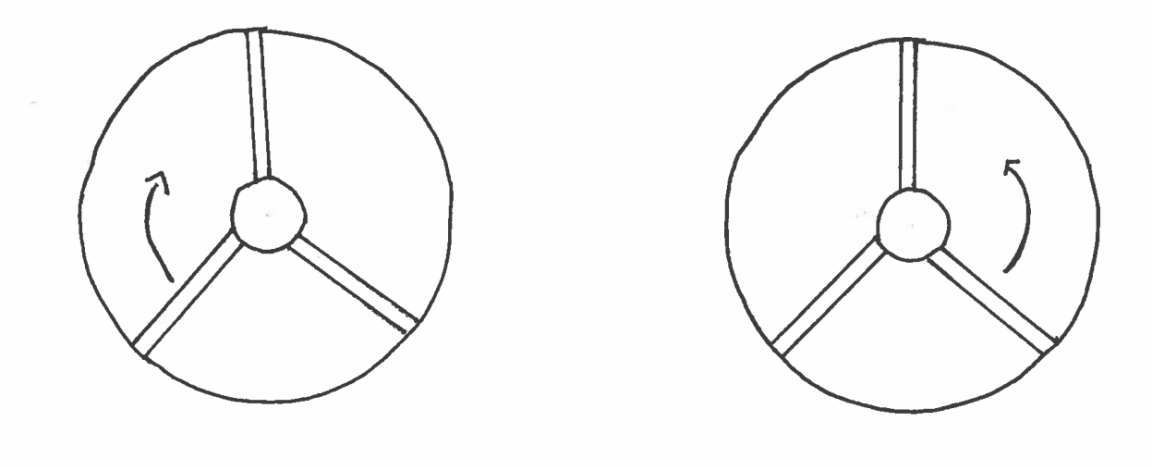

Figure 17: To the left is rotation of the wind turbine for this thesis, to the right is rotation of the wind turbine from previous work.

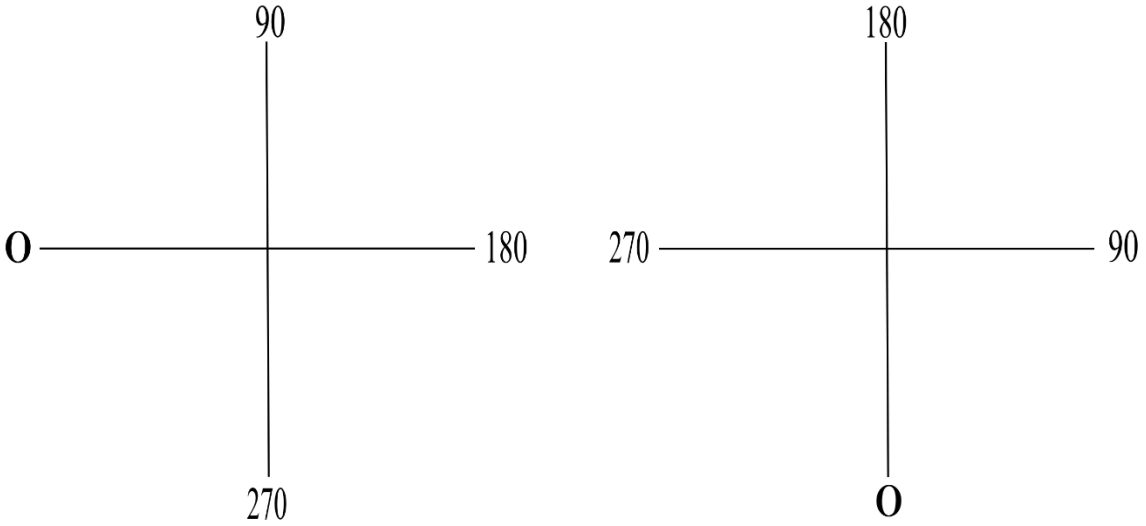

Figure 18: To the left is a set up for angle of rotation for this thesis, to the right is a set up for angle of rotation for previous work.

Table 12: The angle of the blade's position for this thesis correlated to angle of the blade's position in previous work.

Position	This thesis	Correlates	Previous work
1	0°	=	270°
2	90°	=	180°
3	180°	=	90°
4	270°	=	0°

Table 13: Result for deflection in this thesis compared to results from previous thesis.

Position	This thesis (10 m/s)	This thesis (25 m/s)	Correlates	Previous work
1	0.244 m	0.262 m	to	2.202 m
2	0.254 m	0.252 m	to	1.729 m
3	0.243 m	0.244 m	to	1.255 m
4	0.254 m	0.254 m	to	1.728 m

6. Conclusion

To understanding ice shedding from wind turbine blades, this report has focused on horizontal-axis wind turbines. Information concerning properties of ice and how it forms on the blade has been documented. Reason for this being important is due to how ice affects the energy production as well as potential risk caused by ice throw. Ice accretion on wind turbine blades are caused by either precipitation icing or in-cloud icing. However, indications shows the wet snow, which is from precipitation icing, falls almost instantly of the wind turbine blade. Covering the meteorological conditions for ice growth gives insight to what type of ice accretion forms on the wind turbine blade and by what parameters.

The deformation of atmospheric ice have three influential factors, which also support the recrystallization mechanism of ice. The elastic and plastic deformation happens when forces are applied, whereas elastic deformation are the dominant one and plastic are virtually non-existent. The two other factors where displacement of crystals with respect to each other and destruction of ice crystals. These three factors also have a correlation with adhesive properties of ice, which explains how ice sticks to the surface of the wind turbine blade. By understanding the adhesive strength of ice, an estimate of how much shear force, tension strength and weight the ice can withstand before it sheds is possible.

The numerical analysis was by Ansys by importing a CAD-file of the wind turbine blade model made in Inventor. By using finite element method in Ansys, simulations of deflection on the blade was done. However, by looking at the results in Table 8 and 9 there are deficits in the analysis. The writer have unfortunately not been able to unveil the reason for these results despite several attempts. Probable cause may have to do with setup in Ansys or parameters that are not correct. Results from previous work has been listed in Table 11 and a correlation of the blades position through its rotation for this thesis and from previous work has been listed in Table 12. In position 1 for the blade for this thesis, it is expected that the blade have its highest deflection. The blade, in position 1, has the load from the wind and the standard earth

gravitational force to press the blade downward while the rotational velocity is rotating the blade in opposite direction. Position 2 and 4 are not as affected by the standard earth gravity due to it either compress the blade, or stretch the blade in this position. The deflection should mainly come from wind resistance working against the wind turbine blade due to the rotational velocity. The least deflection should be in position 3, where rotational velocity acts in the same direction as the standard earth gravity, however, the wind resistance acting on the wind turbine blade should decrease the deflection.

Taking in consideration that ice throw does not occur suddenly, but built up over time, there are several factors concerning this phenomenon. Factors such as the elastic and plastic deformation, brittle fractures, creep, porosity, temperature, salinity and adhesive strength.

By looking at results from previous work, the maximum deformation happens at 270° throughout the rotation. At this position, maximum forces acts on the wind turbine blade and contributes most to ice shedding.

6.1. Future work

Future work based on this report should be to have successful analysis of directional deformation, as well as how stresses and forces affects the wind turbine blade. Model used for this report is a rough estimation of it geometry and is simulated as a solid in E-glass fiber. For a more detailed analysis of a wind turbine blade, dimensions used for an actual wind turbine blade should be used with materials used in the construction of the blade. In addition, get better understanding of the mechanical properties and behavior of atmospheric ice.

7. References

[1] Statkraft, "Vindkraft," [Online]. Available: https://www.statkraft.no/Energikilder/Vindkraft/. [Accessed 18 January 2019].

[2] N. A. Johnsen and A. N. Trygstad, "NRK," NRK, 28 April 2018. [Online]. Available: https://www.nrk.no/nordland/investeringer-i-vindkraft-har-okt-med-over-400-prosent-1.14012737. [Accessed 18 January 2019].

[3] K. Fredriksen, "Statistisk sentralbyrå," Statens Sentral byrå, 27 August 2018. [Online]. Available: https://www.ssb.no/energi-og-industri/artikler-og-publikasjoner/vindkraft-oker-mest. [Accessed 18 January 2019].

[4] K. M. Hovland, "E24," 7 September 2018. [Online]. Available: https://e24.no/energi/det-groenne-skiftet/utenlandske-milliarder-til-norsk-vindkraft-vi-liker-norden/24435303. [Accessed 18 January 2019].

[5] U.S. Energy Information Administration, "Types of Wind Turbines," 19 December 2018. [Online]. Available: https://www.eia.gov/energyexplained/index.php?page=wind_types_of_turbines. [Accessed 21 January 2019].

[6] R. Smith, "Symscape," 4 June 2007. [Online]. Available: https://www.symscape.com/blog/vertical_axis_wind_turbine. [Accessed 21 January 2019].

[7] Vindportalen, "Vindportalen," [Online]. Available: https://www.vindportalen.no/Vindportalen-informasjonssiden-om-vindkraft/Vindkraft/Cold-climate-English/Weather-condition-and-different-types-of-icing. [Accessed 19 February 2019].

[8] P. Sokolov, "Analysis of ice Shedding," Department of Computer Science and Computational Engineering, Narvik, 2017.

[9] The Editors of Encyclopedia Britannica, "Encyclopedia Britannica," 20 July 1998. [Online]. Available: https://www.britannica.com/science/glaze#ref44530. [Accessed 19 February 2019].

[10] S. S. Haaland, "Estimating Production Loss due to Icing on Wind Turbines," University of Tromsø, Tromsø, 2011.

[11] The Editors of Encyclopedia Britannica, "Encyclopedia Britannica," 28 July 1998. [Online]. Available: https://www.britannica.com/science/rime-weather. [Accessed 19 February 2019].

[12] Diffen, "Adhesion vs. Cohesion," [Online]. Available: https://www.diffen.com/difference/Adhesion_vs_Cohesion. [Accessed 5 March 2019].

[13] Biology Dictionary, "Adhesion Definition," [Online]. Available: https://biologydictionary.net/adhesion/. [Accessed 5 March 2019].

[14] The U.S. Geological Survey, "Adhesion and Cohesion of Water," 17 July 2018. [Online]. Available: https://water.usgs.gov/edu/adhesion.html. [Accessed 5 March 2019].

[15] M. C. Homola, "Atmospheric icing on wind turbines," Norwegian University of Science and Technology, Trondheim, 2011.

[16] American Meterological Society, "Translation of the Mechanical Properties of Ice," The American Meterological Society, Boston, Massachusetts, USA, 1960.

[17] H. H. G. Jellinek, "Adhesive Properties of Ice," U. S. Army Snow Ice anad Permafrost Research Establishment, Wilmette, Illinois, 1959.

[18] R. Scavuzzo and M. Chu, "Structural Properties of Impact Ices Accreted on Aircraft Structures," The University of Akron, Akron, Ohio, 1987.

[19] Q. Wang, "Ice-induced vibrations under continuous brittle crushing for an offshore wind turbine," Norwegian University of Science and Technology, Trondheim, 2015.

[20] H. Hendrikse and A. Metrikine, "Ice-induced vibrations and ice buckling," Elsvier B.V., Amsterdam, Netherland, 2016.

[21] N. Davis, A. N. Hahmann, N.-E. Clausen and M. Zagar, "Forcast of icing events at a wind farm in Sweden," Journal of Applied Meteorology and Climatology, Aarhus, Denmark, 2013.

[22] Nordkraft, "Nordkraft," CoreTrek, [Online]. Available: https://www.nordkraft.no/kraftverk/nygardsfjellet-vindpark-article368-110.html. [Accessed 27 February 2019].

[23] J. A. Grande, "Plastics Technology," Gardner Business Media, Inc, 10 January 2008. [Online]. Available: https://www.ptonline.com/articles/wind-power-blades-energize-composites-manufacturing. [Accessed 14 May 2019].

[24] L. Thomas and R. M, "Advanced materials for wind turbine blade," ScienceDirect, Bengahuru, 2016.

[25] "Chapter 1: Classification of Materials," [Online]. Available: http://www.uotechnology.edu.iq/dep-laserandoptoelec-eng/branch/lectures/solid%20state/chapter%201%20classification%20of%20materail.pdf. [Accessed 15 May 2019].

[26] B. Eker, A. Akdogan and A. Vardar, "Using of Composite Material in Wind Turbine Blades," 2006. [Online]. Available: https://scialert.net/fulltextmobile/?doi=jas.2006.2917.2921. [Accessed 15 May 2019].

[27] "Automated Dynamics," [Online]. Available: http://www.automateddynamics.com/article/thermoplastic-composite-basics/types-of-thermoplastic-composites/continuous-fiber-reinforcements. [Accessed 15 May 2019].

[28] AZoM.com, "AZO Materials," AZoNetwork, 30 August 2001. [Online]. Available: https://www.azom.com/article.aspx?ArticleID=769. [Accessed 23 May 2019].

[29] Institut National Des Sciences Appliquées, "Aerodynamic Forces," [Online]. Available: https://moodle.insa-lyon.fr/pluginfile.php/40040/mod_resource/content/1/wrenches/Aerodynamic_Forces_Drag_Lift-Thrust.pdf. [Accessed 19 March 2019].

[30] D. Wood, "Gravitational Force: Definition, Equations & Examples," study.com, [Online]. Available: https://study.com/academy/lesson/gravitational-force-definition-equation-examples.html. [Accessed 19 March 2019].

[31] J. Lucas, "What Are Centrifugal & Centripital Forces?," Live Science, 15 October 2015. [Online]. Available: https://www.livescience.com/52488-centrifugal-centripetal-forces.html. [Accessed 19 March 2019].

[32] M. Oak, "Understanding What is Gyroscopic Effect With Appropriate Examples," ScienceStruck, 18 March 2018. [Online]. Available: https://sciencestruck.com/what-is-gyroscopic-effect. [Accessed 20 March 2019].

[33] F. Irgens, Fasthetslære, Trondheim: Tapir Akademiske Forlag, 2006.

[34] Techopedia, "Autodesk Inventor," Techopedia Inc., [Online]. Available: https://www.techopedia.com/definition/24055/autodesk-inventor. [Accessed 27 May 2019].

[35] CAE Associates, "Introduction to ANSYS Mechanical (Workbench)," CAE Associates Inc., [Online]. Available: https://caeai.com/courses/introduction-ansys-mechanical-workbench. [Accessed 27 May 2019].

[36] A. Harish, "Finite Element Method - What Is It? FEM and FEA Explained," Simscale, 24 April 2019. [Online]. Available: https://www.simscale.com/blog/2016/10/what-is-finite-element-method/. [Accessed 27 May 2019].

[37] Autodesk, "Node and Elements," [Online]. Available: http://download.autodesk.com/us/algor/userguides/mergedprojects/Getting_Started/introduction_to_algor/Nodes_and_Elements.htm. [Accessed 2 June 2019].

[38] Sharcnet, "SOLID187 Element Description," [Online]. Available: https://www.sharcnet.ca/Software/Ansys/17.0/en-us/help/ans_elem/Hlp_E_SOLID187.html. [Accessed 3 June 2019].

[39] Sharcnet, "SURF154 Element Description," [Online]. Available: https://www.sharcnet.ca/Software/Ansys/17.0/en-us/help/ans_elem/Hlp_E_SURF154.html. [Accessed 3 June 2019].

[40] H. Hendrikse and A. Metrikine, "Interpretation and prediction of ice induced vibrations based on contact area variation," Delft University of Technology, Delft, 2015.

[41] H. Hendrikse and A. Metrikine, "Ice-induced vibrations and ice buckling," Delft University of Technology, Delft, 2016.

[42] Top-Alternative-Energy-Sources.com, "Horizontal Axis Wind Turbine," [Online]. Available: http://www.top-alternative-energy-sources.com/horizontal-axis-wind-turbine.html. [Accessed 16 February 2019].

[43] A. K., "Bright Hub," [Online]. Available: https://www.brighthub.com/environment/renewable-energy/articles/92978.aspx. [Accessed 16 February 2019].

Appendix A: Inventor wind turbine blade coordinates

2992,15	260,7445
2564,7	320,5875
2137,25	366,32465
1709,8	395,39125
1282,35	400,9481
1067,795	391,97165
854,9	371,8815
641,175	340,67765
427,45	291,94835
320,5875	259,0347
213,725	216,71715
106,8625	158,58395
53,43125	115,83895
0	0
53,43125	-88,0547
106,8625	-122,2507
213,725	-164,1408
320,5875	-191,07015
427,45	-209,4505
639,1	-231,6779
854,9	-241,9367
1067,795	-243,6465
1282,35	-240,2269
1709,8	-224,41125
2137,25	-199,61915
2564,7	-166,7055
2992,15	-130,37225

Appendix B: Mesh information for DesignModeler

Object Name	*Mesh*
State	Solved
Display	
Display Style	Use Geometry Setting
Defaults	
Physics Preference	CFD
Solver Preference	Fluent
Element Order	Linear
Element Size	Default
Export Format	Standard
Export Preview Surface Mesh	No
Sizing	
Use Adaptive Sizing	Yes
Resolution	Default (2)
Mesh Defeaturing	Yes
Defeature Size	Default
Transition	Slow
Span Angle Center	Medium
Initial Size Seed	Assembly
Bounding Box Diagonal	30,537 m
Average Surface Area	60,509 m²
Minimum Edge Length	0,15443 m
Quality	
Check Mesh Quality	Yes, Errors
Target Skewness	Default (0.900000)
Smoothing	Medium
Mesh Metric	None
Inflation	
Use Automatic Inflation	None
Inflation Option	Smooth Transition
Transition Ratio	0,272
Maximum Layers	5
Growth Rate	1,2
Inflation Algorithm	Pre
View Advanced Options	No
Assembly Meshing	
Method	None
Advanced	
Number of CPUs for Parallel Part Meshing	Program Controlled
Straight Sided Elements	
Number of Retries	0
Rigid Body Behavior	Dimensionally Reduced
Triangle Surface Mesher	Program Controlled
Topology Checking	Yes
Pinch Tolerance	Please Define
Generate Pinch on Refresh	No
Statistics	
Nodes	18783
Elements	105842

Appendix C: Mesh information for static structural analysis

Object Name	*Mesh*
State	Solved
Display	
Display Style	Use Geometry Setting
Defaults	
Physics Preference	Mechanical
Element Order	Program Controlled
Element Size	Default
Sizing	
Use Adaptive Sizing	Yes
Resolution	Default (2)
Mesh Defeaturing	Yes
Defeature Size	Default
Transition	Fast
Span Angle Center	Coarse
Initial Size Seed	Assembly
Bounding Box Diagonal	28170 mm
Average Surface Area	1,6118e+007 mm²
Minimum Edge Length	28,865 mm
Quality	
Check Mesh Quality	Yes, Errors
Error Limits	Standard Mechanical
Target Quality	5,e-003
Smoothing	Medium
Mesh Metric	None
Inflation	
Use Automatic Inflation	None
Inflation Option	Smooth Transition
Transition Ratio	0,272
Maximum Layers	5
Growth Rate	1,2
Inflation Algorithm	Pre
View Advanced Options	No
Advanced	
Number of CPUs for Parallel Part Meshing	Program Controlled
Straight Sided Elements	No
Number of Retries	Default (4)
Rigid Body Behavior	Dimensionally Reduced
Triangle Surface Mesher	Program Controlled
Topology Checking	Yes
Pinch Tolerance	Please Define
Generate Pinch on Refresh	No
Statistics	
Nodes	45960
Elements	28128